

Seamless Operation of a Microgrid Using BESS

During Transition Between Grid-
connected and Stand-alone Modes

B. Naeinian

Technische Universiteit Delft



Seamless Operation of a Microgrid Using BESS

During Transition Between Grid-connected and
Stand-alone Modes

by

B. Naeinian

in partial fulfillment of the requirements for the degree of

Master of Science
in Electrical Sustainable Energy

at the Delft University of Technology,

Supervisor: Asst. Prof dr. ir. L. M. Ramirez Elizondo
Thesis committee: Prof. dr. ir. P. Bauer,
Asst. Prof dr. ir. L. M. Ramirez Elizondo,
Asst. Prof dr. ir. J. L. Rueda Torres

An electronic version of this thesis is available at <http://repository.tudelft.nl/>.

Preface

I would like to thank the DCE&S group of TU Delft, in particular, my committee chair, Professor Pavol Bauer for his engagement in the project and his insightful comments and remarks. Furthermore, I would like to express my deepest gratitude to my supervisor Dr. Laura Ramirez Elizondo for her encouragement, kindness and continuous support throughout the past two years. I would like to thank my Ph.D. supervisor Nils van der Blij for his priceless help, support, and guidance during the project. Last but not least, I would like to thank my family for their understanding and endless love and my friends throughout the entire period of my master study.

*B. Naeinian
Delft, November 2016*

Contents

1	Introduction	1
1.1	Motivation	1
1.2	Scope of the Work	2
1.3	Problem Definition	3
1.4	Research Objective	4
1.5	Research Questions	4
1.6	Contribution	4
1.7	Outline of the Thesis	4
2	Microgrids	7
2.1	Introduction.	7
2.2	Microgrid Modes of Operation	7
2.2.1	Grid-connected Microgrid	8
2.2.2	Islanded Microgrid	8
2.3	Microgrid Control Architecture	8
2.3.1	Primary Control	9
2.3.2	Secondary Control	11
2.3.3	Tertiary Control	12
2.4	Storage Systems in Microgrid Control	13
2.4.1	Batteries	13
2.4.2	Flywheel Energy Storage (FES)	15
2.4.3	Super-capacitor	15
2.5	Energy Storage Configuration	15
2.5.1	Power Electronic Interface for ESS.	16
2.5.2	BESS Inverter Control.	18
2.5.3	Battery Power Management	18
2.6	Microgrid Islanding	19
2.6.1	Local Islanding Detection Techniques	19
3	Microgrid Modeling	23
3.1	Introduction.	23
3.2	Microgrid Overview	23
3.3	Battery Energy Storage System Model.	23
3.3.1	Battery Model	24
3.3.2	Voltage Source Converter.	24
3.4	Grid Model	26
3.5	Cables and Lines	27
3.6	Filters.	28
3.7	Choke.	28
3.8	Load Model	28
3.9	PV Model.	28
3.10	Measurement Process	29
3.10.1	DQ Transformation.	29

3.10.2	The Application of dq0 Transformation on a Balanced Three Phase Voltage	30
3.10.3	Instantaneous Power in dq0 Frame	30
3.10.4	Time Invariant Version of dq0 Transformation	31
4	Control strategy	33
4.1	Introduction	33
4.2	Case Studies	33
4.2.1	Grid-connected Mode Control Strategy	33
4.2.2	Stand-alone Mode of The Operation	38
4.2.3	Transition Mode of Operation	42
5	Results	47
5.1	Introduction	47
5.2	Microgrid in Grid Connected Mode of Operation	47
5.3	Microgrid in Stand-alone Mode of Operation	51
5.4	Microgrid in Transition Between Operations without the Implementation of Dual-controller	53
5.5	Microgrid in Transition Mode Between Operations Modes with Dual-controller Implemented	56
5.6	Evaluation of the Control Scheme	58
6	Conclusions and Future Work	61
6.1	Contributions	61
6.1.1	Microgrid Modeling	61
6.1.2	Control Schemes	62
6.1.3	Control Scheme Verification	62
6.2	Future Work	63
6.3	Concurrent Works	63
	Bibliography	65

1

Introduction

1.1. Motivation

High integration of renewable energy sources (RESs) alongside the emergence of a microgrid concept opens a new door to a sustainable future [1]. However, the intermittent, unpredictable and variable nature of RES power output can affect the reliability of the power systems at large, and micro grids specially. This is mainly due to excessive uncertainty RES producers introduce to system operation. Therefore, the voltage and frequency stability of microgrids with high penetration of RES are emerging research fields that require further work.

One solution to overcome the above-mentioned problems is to utilize energy storage. Energy storage systems can reduce the uncertainty and increase stability of microgrids .

At transmission level, large hydro plants can be considered as viable energy storage for the transmission system. At the demand side, the application of battery energy storage systems (BESS) merged with control system using hierarchical schemes, can provide storage capability to efficiently deal with the stability problems in microgrids [2].

In the context of a CSGrIP project, Li-ion battery technology is identified as a suitable solution because of its long life-time and higher energy density compared to competing technologies, such as Lead-acid batteries.

There are two major operating modes for microgrids: grid-connected mode and islanded mode. In the grid-connected mode, microgrids are connected and allowed to trade power with the larger transmission system, whereas in the islanded mode, they operate autonomously.

High penetration of renewable sources worsens the voltage and frequency stability because of the variations in their power generation. Such a drawback is even more adverse in weak grids such as small microgrids. Therefore the reliability of the microgrids is lower compared to the main grid. The voltage and frequency stability issue and lack of inertia due to the minimum presence of diesel generators make the control of the microgrid super important. Using BESS can improve the stability and security of supply when the microgrid is disconnected from the grid and the output power of DERs can not supply the demand thoroughly. BESS are characterized by their quick response that can easily alleviate the DERs variations. Finding a proper control strategy is a key driver for ensuring a stable operation of microgrids. Controlling the microgrids in an optimum way is investigated in so many research topics and has received much attention in the literature [3–7].

Several issues are important to consider when investigating an optimal control strategy for a stand-alone or grid-connected microgrid such as bi-directional power trade capacity with the main grid, the presence of power electronics, demand side management (DSM) capability as well as the existence of distributed generation (DGs). Each of these factors affects the deci-

sion regarding an adequate control strategy to a different direction. However, what makes this more challenging, is to find a control strategy that enables efficient operation and adequate supply to the sensitive loads when operating in either operating mode as well as during the transition between the two.

High penetration of renewable sources (RES) has increased the uncertainty of the system. The increasing uncertainty challenges the voltage and frequency stability resulted from the intermittent and non-dispatchable nature of RES power generation. Such drawbacks are more severe in weak grids such as small microgrids. Therefore maintaining voltage and frequency stability of is not an easy task to fulfill. One way to overcome this difficulty is deploy Battery Energy Storage Systems (BESS) technologies. Large scale utilization of BESS is proven to improve the stability and security of supply when the microgrid is disconnected from the utility grid and/or when the power output of DERs doesn't suffice demand. BESS are characterized by their quick response and high efficiency. Therefore, they can be used to alleviate the variations in RES units [8].

This thesis investigates possible control strategies that are suitable to apply to battery energy storage systems (BESS) to enable a smooth transition between grid-connected and islanded operating mode in a specific microgrid called CSGriP. Disturbances during intentional and unintentional islanding are taken into account, and a control strategy is proposed for the BESS to ensure a smooth transition with minimum disturbances in voltage and frequency.

1.2. Scope of the Work

The SOPRA (sustainable off-grid power station for rural applications) project is working on a modular, sustainable, off-grid power station for rural applications. The SOPRA microgrid includes renewable energy sources (wind, solar, hydropower), electricity storage (batteries) and back-up diesel power. SOPRA project aims at electrifying rural areas which have no connection or weak connection to the main grid. The SOPRA system consists of invertors, battery packs, and advanced control systems that all together, enable supply and demand matching at a real-time. The compact design of SOPRA provides ample amount of storage capacity for approximately 10000 users in just a 20 ft. Container with low energy consumption [9].

"The Cellular Smart Grids Platform (CSGriP) is an expansion of SOPRA which investigates and develops a grid concept in which at distribution level grid parts operate largely self-sufficiently and self-regulating with local, decentralized generation and the local purchase of energy. This involves relatively low energy storage and new Smart Grid technologies. The grid parts are connected to each other by a backbone (the current medium-voltage power grid) to temporarily be able to exchange energy as necessary. The purpose of the concept is the maximum local matching of supply and demand and the maximum integration of decentralized sustainable energy such as solar-PV, micro-CHPs and wind turbines [10]." The possibility of the connection of the microgrid cell to the main grid and other microgrid cells is considered. Connecting several microgrids together builds a stronger grid and the connection to the main grid improves the voltage stability at the PCC. CSGriP is the successor of SOPRA. CSGriP aims to extend the SOPRA system by adding the possibility of grid connection via an HV or MV backbone. One aim of CSGriP is to reinforce the existing SOPRA to a more cellular shape and make it suitable to be applied in rural areas. In CSGriP project, components are designed to respond according to frequency-power droop curve and voltage-reactive power droop curve [10].

Limiting the application of CSGriP in rural areas dictates minimum usage of ICT infrastructures. To remain consistent with this requirement, microgrid frequency is considered as the only means of communication between cells. As the secondary control is not present in this framework, the frequency of each cell is enforced to stay in the narrow range of 49.5 to 50.5

Hz while operating in the islanded-mode. Note that under such condition; each microgrid cell should be ready to connect to the grid when intended.

Last but not least, a single CSGriP cell should always be ready to connect to the grid and also be able to sustain the loads when it is disconnected from the grid. The connection to the grid should be done by fulfilling the synchronization conditions. The disconnection from the grid could be either intentional or non-intentional. In both cases, control strategies should be implemented in a such a way that minimum disturbance in voltage and frequency is observed in the transition state.

1.3. Problem Definition

One prominent feature of microgrids is their ability to be disconnected from the grid by the use of upstream signals at the point of common coupling (PCC). This state of operation is called islanding. Islanding could be executed due to reliability and economic purposes. For example, in case there is a utility grid disturbance, the microgrid switches to islanded mode to sustain continues supply to its consumers using local distributed energy resource (DER) and battery energy storage systems (BESS). There are two types of islanding modes as follows [11, 12]:

1. Intentional islanding: the purpose of intentional islanding is to isolate the microgrid from the rest of the system during the occurrence of a disturbance, or for maintenance purposes. In an intentional islanding mode, the microgrid should continue to supply adequate power to the load. When connected to the grid, inverters usually work in constant-current control mode to supply the grid with a preset power. When the microgrid is islanded, however, DG inverters should fulfill the transition to constant voltage control model [13].
2. Unintentional islanding: "Unintentional islanding happens when the DGs are injecting power to the utility grid when the power from the central utility source has already been discontinued [13]." Unintentional islanding can pose severe challenges to the system as it can easily lead to loss of synchronization. It can also cause DGs to deviate from their nominal voltage and frequency references and/or, damage the electrical equipment in the islanded microgrid [13].

In both occasions, the main objective of the master controller of the microgrid would be to maintain the frequency and voltage within allowed limits. In an ideal case, regardless of the type of the islanding mode, the islanded microgrid could be re-synchronized with the main grid after the disturbance is removed. In addition, during the transition between grid connected and islanded modes, that variations could occur in the magnitude of the voltage and the frequency of the voltage at the PCC. Therefore, the stability of microgrid in the transition state is of great importance in microgrid studies.

As outlined above, ICT infrastructure is rather inadequate in rural areas. Therefore, we consider frequency as the only means of communication between cells within the CSGriP project. To ensure full functionality of CSGriP, SOPRA cells should send frequency signals via backbone line that connects SOPRA cells. During the transition between islanding and grid-connected modes, the SOPRA cells should interact with each other via the backbone to maintain the frequency and continues feed to the loads. Note that each SOPRA cell should be able to connect to the grid when intended. It should also be able to disconnect from the grid at any point in time, regardless of whether it is intended or not. However, there is a need for control strategies that clears the disturbances during transition from grid-connected mode to the stand-alone mode, before the protection relays trip and disconnect the loads.

The quest to realize microgrids demands an adequate control strategy that considers such challenges and addresses them properly.

1.4. Research Objective

The objective of this thesis is to investigate the development of control strategies that can quickly clear the disturbances during transition from grid-connected mode to the stand-alone mode and restore the system to a (semi-normal) operating state, before the protection relays trip and disconnect the loads.

1.5. Research Questions

In the context of this research, my goal is to address the following three research questions:

1. What voltage and frequency disturbances the microgrid would face during intentional and unintentional islanding of CSGriP?
2. What is the adequate control strategy to implement in the BESS during the transition between grid-connected and islanding operating modes?

1.6. Contribution

This research work provides the three following contributions:

- Defines a control strategy for the grid-connected and stand-alone operation of a microgrid using BESS.
- Proposes a methodology to combine the two aforementioned control strategies to enable a smooth transition between one microgrid (e.g., SOPRA) and the main grid during unintentional islanding, under the assumption of no involvement of ICT infrastructure.
- Shows the effectiveness of the proposed approach using numerical simulations.

1.7. Outline of the Thesis

The work in this thesis is structured as follows:

- Chapter 1 introduces the problem by reviewing the literature. It also formulated the research objectives, and enumerated the scientific contributions of this study.
- Chapter 2 provides a comprehensive overview of different topics covered in this thesis, which are: main microgrid architectures, control of the microgrids in a hierarchical way, different energy storage technologies, various islanding detection techniques.
- Chapter 3 proposed a Simulink model for a microgrid as a test subject for implementing the control strategies which are defined in Chapter 4. It is followed by explaining our approach to incorporate energy storage systems into the problem formulation.
- Chapter 4 defines control strategies for three case studies that are defined. The control strategies are demonstrated to ensure stable operation during and smooth transition of the microgrids from the grid-connected mode to the islanded mode.
- Chapter 5 explains the simulation results of the three case studies.

- Chapter 6 summarizes the main conclusions of the thesis and identifies some avenues for further research.

2

Microgrids

2.1. Introduction

This chapter starts with giving an overview of the operational modes of a microgrid. The necessity of the control of the microgrid parameters such as voltage and frequency is justified in each mode of the operation of the microgrid. Three main levels of control architecture in microgrids, are indicated, and the difference between them is discussed. The importance of controlling the battery storage energy systems is elaborated, and the main power electronic interface required to control battery banks is presented. Lastly, the methods to detect microgrid islanding are mentioned which are critical for switching between control strategies for the two modes of operation in a microgrid.

2.2. Microgrid Modes of Operation

“Regardless of the microgrids mode of operation, i.e., 1) grid-connected, 2) islanded (autonomous), or 3) transition between the two modes, the adopted power management system (PMS) has a direct impact on the system operational behavior regarding voltage/angle stability, power quality, and availability of service to consumers.” [14]. The DG units can be considered as reserve sources in the scope of conventional power systems. However, they cannot be considered as reserve sources to produce electricity in the scope of microgrids [14]. The DG units supply the reference power which is dictated by the primary control when they are connected to the grid. The reference power is determined in such a way that there is minimal power injection to the microgrid from the grid side. Each DG can provide the predefined power and let the voltage at the PCC to be imposed by the main grid. If the DG units can not supply the demand thoroughly, the deficit power is supplied by the main grid. In this operation mode, the stabilization of the microgrid voltage and frequency at the PCC is done by the utility grid [14].

When the microgrid is disconnected from the utility grid subsequent to an islanding, the demand should be supplied by the sum of the DG units power generation and the power out of the storage system. The DG units require participating in stabilizing the microgrid voltage and frequency in this operation mode. Fast control schemes should be applied on the DG and BESS inverters to ensure a stable voltage at the PCC. In transition state the voltage dynamics should be alleviated by the DG inverters. In the microgrid with the minimum presence of ICT, the PMS should operate based on the available local information like frequency and voltage magnitude [14].

The main objectives to be fulfilled by PMSs in an islanded microgrid are as follows:

- Share the loads among available DG units and minimize power loss in the microgrid.
- Observe the characteristics of DG units like the type of DG resource, generation cost, maintenance interval, and environmental impact.
- Maintain power quality by limiting the fluctuations in the voltage.
- Improve the dynamic response, maintain the stability margin, and restore the magnitude and frequency of the voltage during and after transients [15].

2.2.1. Grid-connected Microgrid

When the microgrid is connected to a stiff grid, the voltage at the PCC is imposed by the corresponding grid. The prominent objective of a microgrid in this operation mode is to regulate the active and reactive power generated by the distributed energy resources (DERs) and to supply the demand. Reactive power generated by a DER unit can be used to correct the power factor or to control the voltage at the corresponding point of coupling [16].

The DERs in the proximity of PCC should not utilize an active voltage control scheme to minimize the interference with the control scheme of the main grid to stabilize the voltage. Furthermore, The DER units with low power generation capacity are not able to support a utility grid. In other words, utility grid does not allow strict voltage control schemes that are implemented in the inverter controller of the DGs when the microgrid is connected to the main grid [16].

2.2.2. Islanded Microgrid

The microgrids operate in the grid-connected mode most of the time. However, they should operate as a standalone grid when they are disconnected from the utility grid whether it is intentional or unintentional. Under islanded mode, the microgrid should be stable and work autonomously like the way physical islands operate when there is a disconnection from the upstream medium voltage (MV) grid [17].

The present micro sources in a microgrid can not be connected to the AC side of the microgrid without any means of power electronic interface due to the fluctuating nature of power produced by renewable DERs caused by intermittent wind speed and solar irradiation. Thus, power electronic interfaces are necessary to regulate output power produced by DERs and also to bridge the DC side to the AC side. Contrary to the operation in the grid-connected mode of the microgrid, the main objective of the control strategies in islanded mode of a microgrid is to regulate the voltage at the desired level at the PCC since the voltage is not forced anymore by the connection to the upstream medium voltage grid [17].

2.3. Microgrid Control Architecture

The terminal voltage of the synchronous generator can be adjusted using tuning the excitation current using an automatic voltage controller. However, an induction generator is more favorable because of its price, robustness and simpler starting. Different control strategies are used to modify the magnitude and frequency of the voltage in the presence of induction and synchronous generators. In an islanded microgrid, the fluctuations in active power change the frequency of the microgrid. The surplus power in an autonomous MG should be dissipated in dump loads or stored in storage devices like batteries or flywheels [18].

In conventional power systems, there are three levels of control: Primary control, Secondary control and Tertiary control [19]. The same three types of control are utilized to control microgrids. The difference among these three levels is in their response time. The required

infrastructure such as communication infrastructure is also a differentiating factor among different levels of control [16].

- Primary control: The first level of control that has the fastest response time is called the primary control. The primary control senses the dynamics in the microgrid system and responds to the variations in the voltage and the frequency [20]. This control level captures the available local signals like the voltage magnitude and frequency and tries to damp the error between the measured variables and their references by using linear control schemes. Islanding detection and changes in the modes of the controller lie in the objectives of primary control because of its fast response [16].
- Secondary control: The secondary control guarantees the power quality and alleviates the deviation of frequency and magnitude of the voltage from the desired level subsequent to the primary control. The secondary control determines the new set points for the primary control to achieve its objectives [16]. The response time of the secondary control is in the order of on minute which is much slower than the response time of the primary control. The primary control has already reached its steady state prior to the response of the secondary control to change the set points. Therefore, the secondary control is decoupled from the primary control. The secondary control needs a low bandwidth to measure the microgrid variables. Therefore a communication link is required to implement the secondary control [16].
- Tertiary control: The tertiary control is one level higher than the secondary control. The tertiary control is slower than the secondary control and determines the steady state set points by using the optimal power flow requirements. The tertiary control needs higher investment in communication infrastructure as it requires to get information from the DG units, market, and other system requirements [16].

2.3.1. Primary Control

The goal of control schemes implemented in a microgrid operating in the islanded mode is to balance the supply and demand within an acceptable range of frequency and voltage [18].

The primary control in microgrids should enable the parallel inverters to share the loads. To share the loads among parallel inverters, one can use the droop control method that is derived from the concept of droop controllers implemented in conventional power grids. Another method that can be used to share the loads in parallel inverters is to use the virtual impedance method. However, the droop method is more conventional in this regard [21].

There are mainly two control strategies applied on inverters in a microgrid. PQ inverter control and voltage source inverter (VSI) control.

- PQ controlled inverter sets the active and reactive power that is going to be supplied to the load based on a given value.
- Voltage source inverter (VSI) control provides the load with defined set-points of the magnitude and the frequency of the voltage. Therefore, the reactive and active power input to the load is based on the load itself.

The PQ inverter injects the reactive power based on a pre-defined value. This value is either specified locally by local control loops or centrally by a microgrid central controller (MGCC). The PQ inverter control acts as a current controlled voltage source whereas, the VSI resembles the operation of synchronous machines in power system. The synchronous machines are used to control the magnitude and frequency of the voltage, and the VSI wants to mimic

such a behavior [22]. The VSI can be considered as a voltage source, the magnitude and the frequency of the voltage is controlled based on the slope of droop curves. The following equations show how voltage and frequency are being controlled [23].

$$\omega = \omega_0 - K_P \times P \quad (2.1)$$

$$V = V_0 - K_Q \times Q \quad (2.2)$$

$$K_P = \frac{f_{\max} - f_{\min}}{P_{\max}} \quad (2.3)$$

$$K_Q = \frac{V_{\max} - V_{\min}}{Q_{\max}} \quad (2.4)$$

where P and Q represent the output active and reactive power of the inverter respectively, K_P and K_Q represent the slopes of the active power-frequency and reactive power-voltage droop curves, and ω_0 and V_0 represent the values for the angular frequency and the terminal voltage of the inverter when it operates without any load connected to it [24].

When a VSI is interfaced with a stiff utility grid, which has a constant angular frequency and voltage represented by ω_g and V_g respectively, the magnitude and the frequency of the terminal voltage references are externally dictated [24].

There are mainly two control strategies for controlling the islanded microgrid.

- A single master operation: One VSI sets the voltage reference for all the other inverters. The inverter which sets the voltage is called master and the other inverters which follow the master are called the slaves. The slave inverters operate in PQ operation mode.
- A multi-master operation: The multi-master operates with several VSIs, each has its voltage and frequency characteristic.

Power Control in Parallel DERs

In order to share the power in an appropriate way between the DER units, the "Plug and Play" characteristic as a common feature could be utilized. A droop characteristic is used to control the power sharing among inverters withing accepted voltage and frequency margins. (IEC 60038, 380V with +10 percent and -6 percent at 50Hz +0.5 -0.5Hz) [25].

Figure 2.1 shows a sample DER connected to the PCC in an islanded microgrid by the line impedance of Z , inverter voltage of E and V as the voltage of PCC. δ_E and δ_V are phase angles of E and V respectively. If the resistance of the connecting line is not considered, the flow of active and reactive power can be represented in Equation 2.5 [25].

$$P = \frac{EV\sin(\delta_E - \delta_V)}{X} \quad (2.5)$$

$$Q = \frac{V^2 - VE\cos(\delta_E - \delta_V)}{X} \quad (2.6)$$

If we consider that the $(\delta_E - \delta_V)$ is small enough, the active power which is transferred by the line is proportional to $(\delta_E - \delta_V)$, and transferred reactive power is proportional to the difference in voltage magnitude $(V - E)$. Therefore, the angle difference and thus the frequency can control the inverter active power and the voltage can control the reactive power which is produced by the inverter [25].

The inverter operates in the limitation range of the magnitude and frequency of the voltage to balance the active and reactive power in islanded operation [25]. ("the experimental results

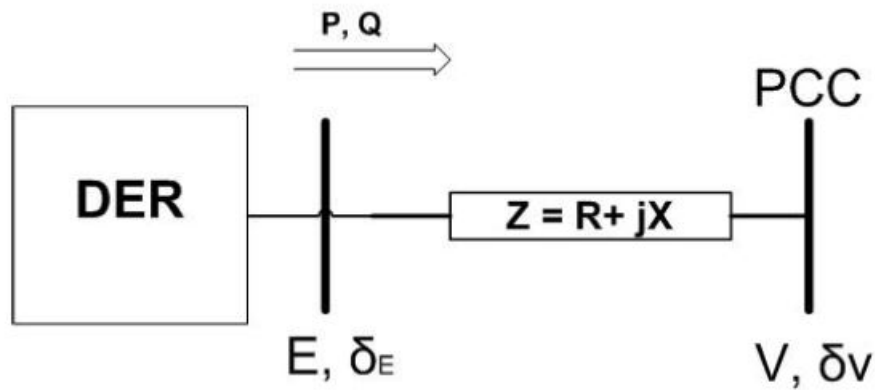


Figure 2.1: A distributed energy resource (DER) is connected through an impedance to the PCC [25].

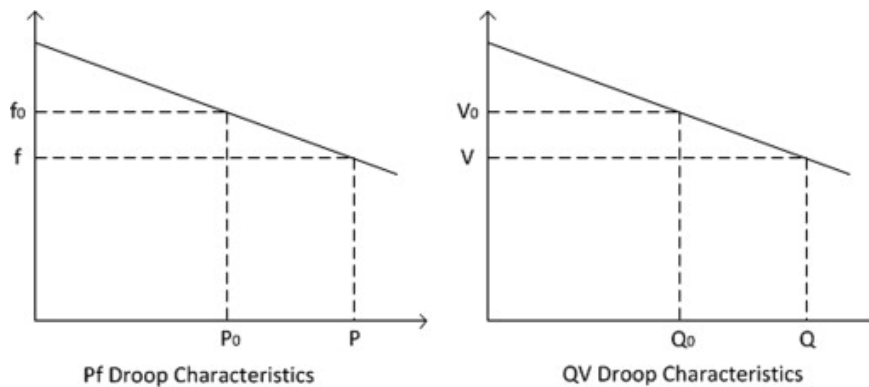


Figure 2.2: Frequency/active-power and voltage/reactive-power droop curves representation [26].

show that the output voltages of the sources controlled by a VSI controller are stable during load variations whereas their active and reactive powers change significantly. On the contrary, the PQ controller keeps the output power of the controlled source constant, but its output voltage varies according to the load. This study shows that both controllers are effective, but one alone cannot control the whole parameters of an MG." [25])

There are two main control strategies: central control strategy and peer to peer strategy. In peer to peer strategy, every micro source (MS) is responsible for ensuring the power quality which is delivered to the grid. This kind of strategy is more desirable because there is no need for communication between the sources. New MSs can be added to the MG without changing the control strategy [18].

2.3.2. Secondary Control

The primary control finds new set-points for the magnitude and the frequency of the voltage to supply the required active and reactive power. Therefore, there are some deviations between the reference values of the voltage and frequency and their measured values after the implementation of the primary control. The secondary control tries to damp these deviations in voltage and frequency. This stage of hierarchical control guarantees the voltage and frequency variations are compensated subsequent to any change in the microgrid. The frequency and voltage value are monitored and compared to their reference values. The errors are calculated and injected into the corresponding compensators and then are dispatched to all micro source (MS) controllers to recover the magnitude and frequency of the voltage [27]. The secondary control ensures that the magnitude and the frequency of the voltage are within

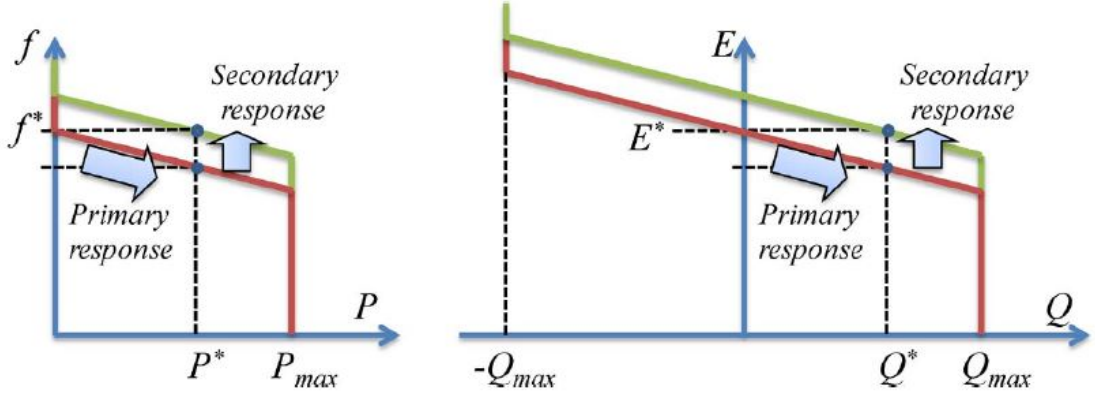


Figure 2.3: Primary and secondary controls based on droop curves of frequency/active power and the voltage/reactive power [29].

desirable limits. The allowed range for Nordel (north of Europe) is 49.9 Hz to 50.1 Hz and the desirable range for UCTE (Continental Europe) is 49.8 Hz to 50.2 Hz [28].

The secondary control consists of proportional integral derivative (PID) controllers in Europe or utilize automatic gain controllers in the US. The controllers which are used to restore the voltage and frequency can be designed based on the following equations [28].

$$\delta_f = K_{pf}(f_{MGref} - f_{MG}) + K_{if} \int (f_{MGref} - f_{MG})dt + \Delta f_s \quad (2.7)$$

$$\delta_V = K_{pV}(V_{MGref} - V_{MG}) + K_{iV} \int (V_{MGref} - V_{MG})dt \quad (2.8)$$

where K_{pf} , K_{if} , K_{pV} , and K_{iV} represent the parameters for the compensators which are implemented in the secondary control and Δf_s is the term that represents the synchronization criteria which is zero when there is no connection to the utility grid. δ_f and δ_V should be in desirable limits when the microgrid operates in stand-alone mode.

In Figure 2.3, the primary and secondary control actions are depicted based on $P - F$ and $Q - V$ characteristics. In a microgrid controlled through droop curves, secondary control shifts the Pf and QV curves so as the magnitude and the frequency of the voltage are drifted toward their nominal values.

2.3.3. Tertiary Control

When the microgrid operates in the grid-connected mode of operation, the flow of power from the grid side to the microgrid side can be controlled by changing the frequency and the magnitude of the voltage in the microgrid at the PCC. By monitoring active and reactive power at PCC, the flow of power can be controlled based on following equations.

$$f_{MGref} = K_{pP}(P_{Gref} - P_G) + k_{iP} \int (P_{Gref} - P_G)dt \quad (2.9)$$

$$V_{MGref} = k_{pQ}(Q_{Gref} - Q_G) + k_{iQ} \int (Q_{Gref} - Q_G)dt \quad (2.10)$$

where k_{pP} , k_{iP} , k_{pQ} and k_{iQ} are the parameters of control in tertiary control compensator. The

f_{MGref} and V_{MGref} will be saturated if they are outside of the desirable limits. In islanded mode f_{MG} and V_{MG} are controlled to be equal to f_{MGref} and V_{MGref} respectively by secondary control. When the microgrid operates in the grid-connected mode, the synchronization procedure can begin and f_{MGref} and V_{MGref} will be equal to grid values. Therefore the reference values for the magnitude and the frequency of the voltage is equal to the magnitude and the frequency of the voltage of utility grid. When the synchronization is done, f_{MGref} and V_{MGref} can be given by Equation 2.9 and Equation 2.10. The active and reactive power can be controlled in a decoupled way base on the sign of the reference values for P_G and Q_G . The interchange of P and Q are depicted based on tertiary control in Figure 2.4.

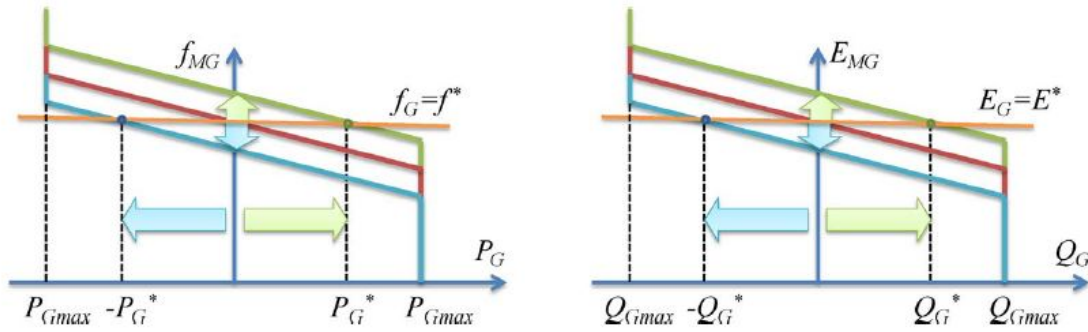


Figure 2.4: Tertiary control based on droop curves of frequency/active power and the voltage/reactive power [29].

2.4. Storage Systems in Microgrid Control

The energy storage is usually achieved by stationary units, like different types of batteries, flywheels, etc. The recent development of electrical vehicles (EV) to microgrid/grid connection is promoting the idea of considering EVs as energy storage system for future [30].

The frequency stability is of major concern in a islanded microgrid. One of the most talked about solutions (discussed) to tackle this problem is to improve the frequency stability using energy storage systems [31]. In the scale of conventional power systems, pumped hydro power plants could be a desirable solution; however, utilizing BESS together with the hierarchical control of RESs is a more feasible way to tackle the frequency and voltage variations in the scale of microgrids [31].

2.4.1. Batteries

Batteries store energy in the form of electrochemical energy. The batteries have a wide range of sizes starting from less than 100 W all the way up to several megawatts. The efficiency of batteries is dependent on the type of the electrochemistry materials which are implemented and also the operational cycle and range from 60 to 80% [32]. Lead-acid, Nickel-Cadmium (NiCd), Nickel-Metal Hydride (NiMH), Lithium-ion batteries are the most common type of batteries used in MGs. The energy density of the batteries has continuously increased in recent years. The 2.5 shows the trend since the first lead-acid battery emerged in 1860 [33].

Lead-acid is the most well established and affordable form of battery storage system among all the different technologies; however, the overall economic value of the system is decreased by the limited cycling capability of these batteries. NiCd batteries show higher energy density, lower maintenance cost and longer life cycle compared to lead-acid batteries. NiMh takes the edge in terms having higher energy capacity and being environmentally friendly with having

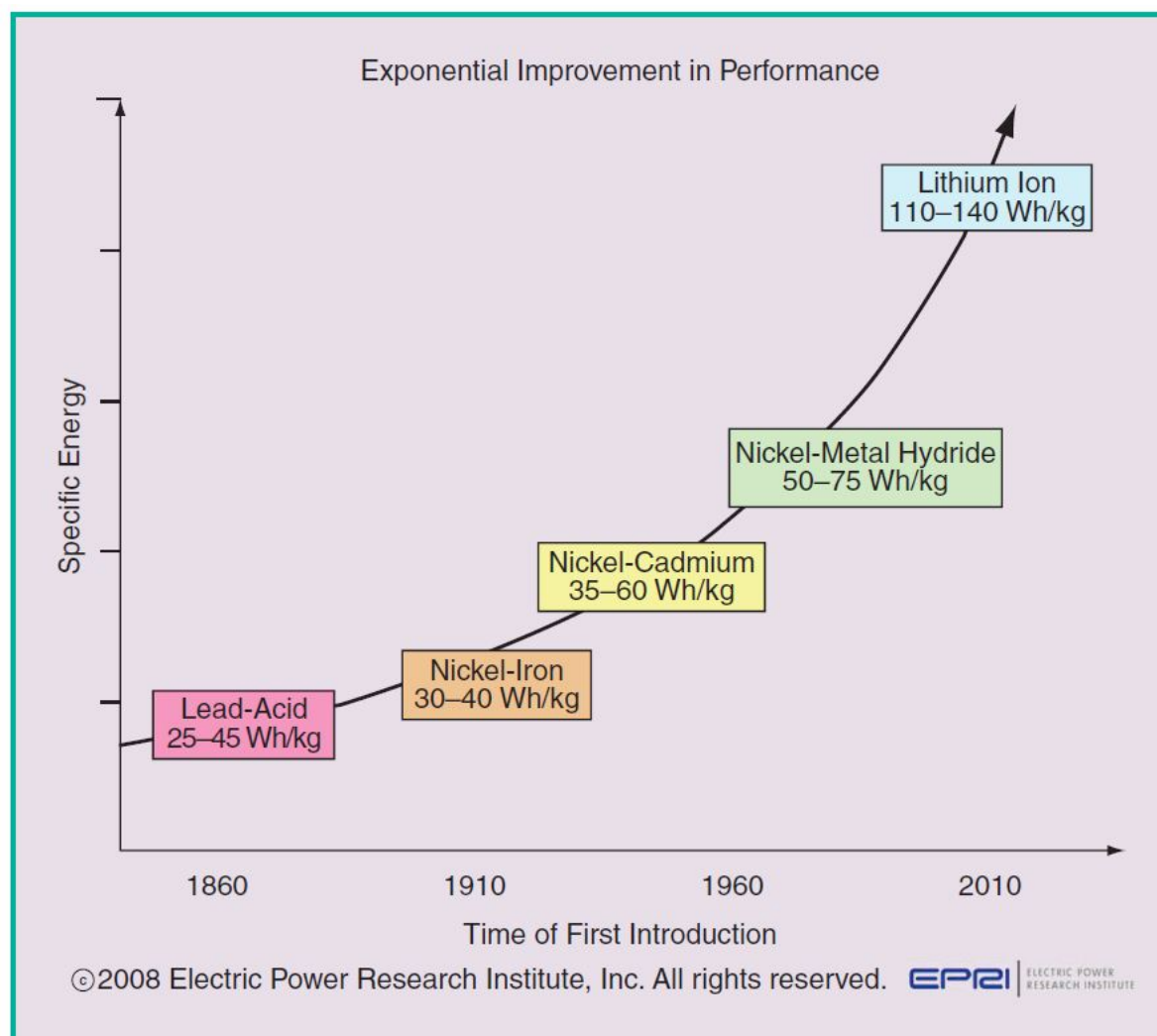


Figure 2.5: Advancements in energy density capacity of various types of batteries through the years [32].

the same life cycle as lead-acid batteries. Lithium ion batteries have the lead regarding capacity; however, their cost is highest amongst the four technologies mentioned [32].

An analysis is done in [34] based on models in Simulink to compare different technologies from a techno-economic point of view. The results suggest that NiMH batteries are the most suitable energy storage technology regarding the power output, voltage profile, and charge/discharge characteristic. The lead-acid batteries show the most affordability compared to other technologies.

There are researches being conducted in modern battery technologies like Sodium-sulfur (NaS) batteries. NaS batteries have already been implemented in numerous projects all around the world. NaS batteries have higher energy densities at much lower cost compared to other more mature technologies. They also show a longer life cycle capability (around 2500 upon 90% depth of discharge) and quick response time in order of one millisecond for a full charge and discharging operation which is ideal to be implemented in MG applications [32]. The cell efficiency of 89% without self-discharge, low maintenance requirements and long cell life of up to 15 years are among other advantages of NaS batteries; however, having a high energy capacity and safe operation in high temperatures can be problematic when using such a technology [35].

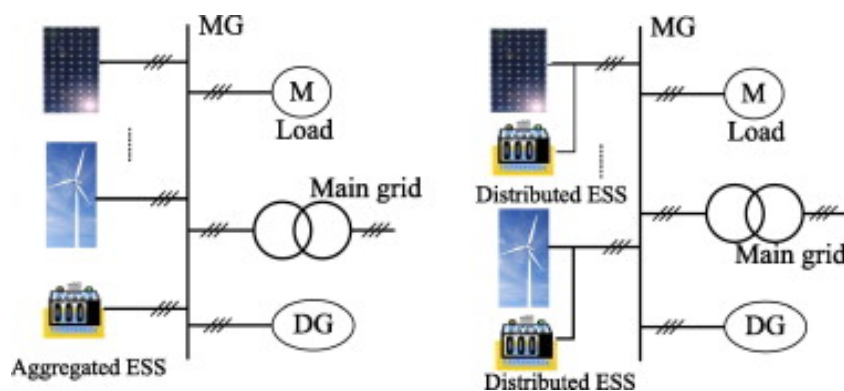


Figure 2.6: Two main topologies (aggregated and distributed) for placing the energy storage systems into a microgrid [32].

China has implemented the first large-scale aggregated energy storage system using NaS technology. This industrial Battery station has the capacity of 100 kW and 800 kWh and is used in world Exp 2010 Shanghai.

2.4.2. Flywheel Energy Storage (FES)

FESs store electrical in the form of rotational kinetic energy. They use electrical energy to rotate a rotor at a very high speed. A FES has a high power density and is considered as an environmentally friendly storage system. The charging and discharging cycles of an FES are practically unlimited, and the rating could go beyond 1000 KW as used in frequency regulation in the USA. The cons of using FESs lies in their limitation in the expansion of their storage, large sizes, and low energy density while having high standby losses [32].

2.4.3. Super-capacitor

Super-capacitors store energy in their capacitors which are arranged in series. The technology which is used is called electric double layer (EDL) that is formed between the ions and the electrodes. The storage of energy is done without any chemical process in between, so the response time of the supercapacitors lower than the batteries. The energy density of the supercapacitors is thousands of time higher than the capacitors utilizing electrolytic technology. Regarding the energy density, they are outnumbered by lead-acid batteries. However, the life time of supercapacitors is tens of thousands of times which is dramatically higher than of the lead-acid batteries. The ability of fast charge and discharge is another advantage in favor of using the supercapacitors. Their characteristics make them a good candidate for a short term energy storage system (ESS) to absorb and release a high amount of energy in a short period [32].

2.5. Energy Storage Configuration

There are two different configurations of energy storage systems (ESSs) that are implemented in microgrids. In the first configuration, the ESSs can be put in a aggregated way. In the second configuration, the ESSs are dispatched in a distributed way. Both configurations can be seen in Figure 2.6. In the first configuration, all ESSs are combined as a single ESS. The aggregated ESS is interfaced with the microgrid, which helps to smooth out the power flow fluctuations at the PCC. The aggregated ESS is considered to have a better response to compensate the variations in voltage and frequency than the distributed ESSs [36], [37].

The ESS in aggregated arrangement is interfaced with the AC side of the microgrid by the help

of an inverter. For interfacing a FES which is coupled with an induction machine, an AC-DC-AC converter should be implemented. A DC-DC converter is used to interface a super-capacitor with the voltage source converter (VSC) that converts the DC voltage to an AC voltage [32].

Increasing the size of aggregated ESS, the cost of manufacturing and control of ESS rise tremendously. Therefore, using distributed configuration makes more sense to ensure flexible and efficient power regulation. The distributed ESSs are connected directly to individual DERs using different interfaces. The advantage of distributed ESS is that the power electronic interface of each pair of ESS and correspondent DER can be controlled and optimized to lower the cost and increase the efficiency. The single source connection to each ESS increase the simplicity of the system and thus the control. The main disadvantage of using such a structure is the power losses increase in both interfaces and line impedance between ESS and the connected DER despite the fact that power electronic interfaces could be optimized separately to minimize the costs. As a result, a hybrid configuration of aggregated model of ESS and distributed configuration of ESS could be a possible solution to optimize the cost and efficiency of the total system [32].

2.5.1. Power Electronic Interface for ESS

The ESS converter is used continuously compared to other converters in the microgrid that only operates when the primary source of energy is available. The continuity of support to the microgrid requires high reliability and efficiency in the chosen converter topologies for ESS [38].

The primary objective of the BESS is to gain the control of the flow of power between the battery banks and the microgrid terminal. To achieve this objective, the voltage level of the battery banks should be adapted according to the microgrid. The DC voltage of the battery banks is between 12-120 V for power is the range of several tens of kW. The higher the voltage levels in battery banks, the simpler the VSC can adapt to the voltage at the AC side of the microgrid and the higher the efficiency of the converter [21].

The converter operates in two stages: the first step takes care of the conversion of DC to AC, and the next stage increases the magnitude of the voltage to match the microgrid AC voltage level. Based on the structure of the converters these two steps are fulfilled by various configurations. Two common architectures for the power electronic interfaces in BESS are depicted in Figure 2.7. The inverter stages of the two configurations are similar while the main difference is in the boost up stage [21].

In the first configuration, a bi-directional DC-DC converter is implemented between the DC bus and the transformer. The transformer which is used in this configuration has the frequency in the order of tens of kHz. The implementation of such a configuration is costly because of the presence of both a DC-DC converter and an inverter. The capacitor in the DC bus is quite large to alleviate the fluctuations in the single phase system. One of the disadvantages of using such a structure is the short life time of the electrolytic capacitor. The structure provides a decoupled control of the power which is transferred to the AC side and the battery side [21].

The lack of the presence of the transformer on the microgrid side allows the flow of a DC current component, which exerts additional thermal stress on some equipment in the microgrid. Therefore, an extra current loop is required to decrease the DC component of current under a certain level [39].

The second configuration allows the battery to connect to DC link without any converter in between. A 50 Hz transformer increases the voltage to the MG level. This configuration is simpler than the first one while the efficiency is lower due to the transformer. The transformer increased the earth leakage current, requiring extra consideration in differential protection system [21].

Contrary to the first configuration, the power flow injected into the battery and the inverter cannot be controlled independently because of the direct connection of the two components without any transformer in between. As a result, the battery bank current includes both DC and AC components with twice the grid frequency in the presence of the nonlinear loads. These components in the current would decrease the life time of the battery [21].

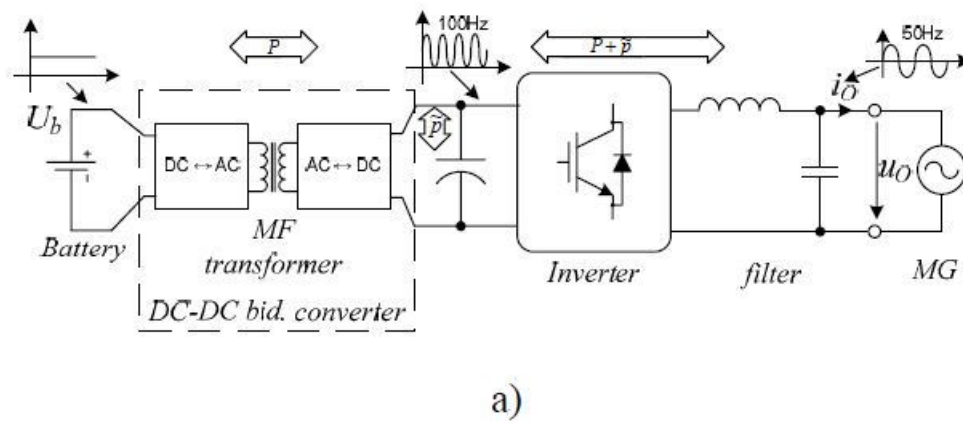


Figure 2.7: First battery converter topology including a bidirectional DC-DC converter [21].

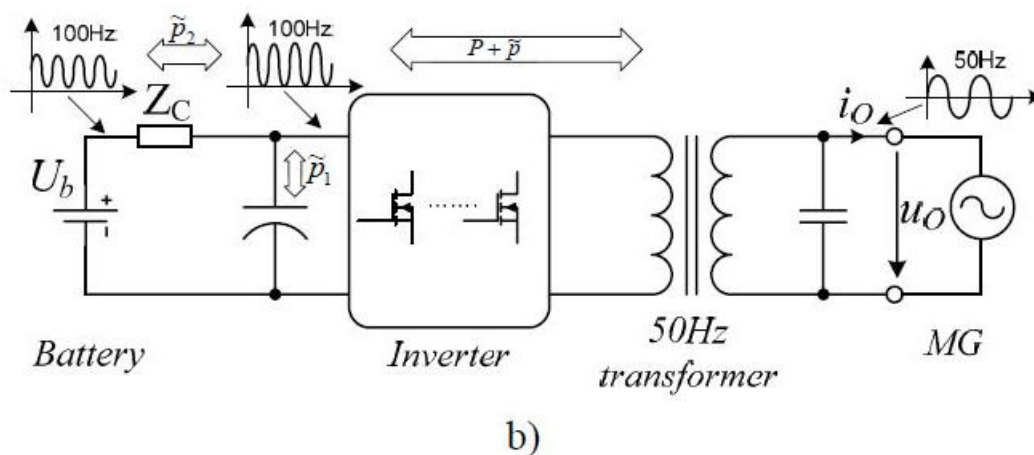


Figure 2.8: Second battery converter topology including a transformer [21].

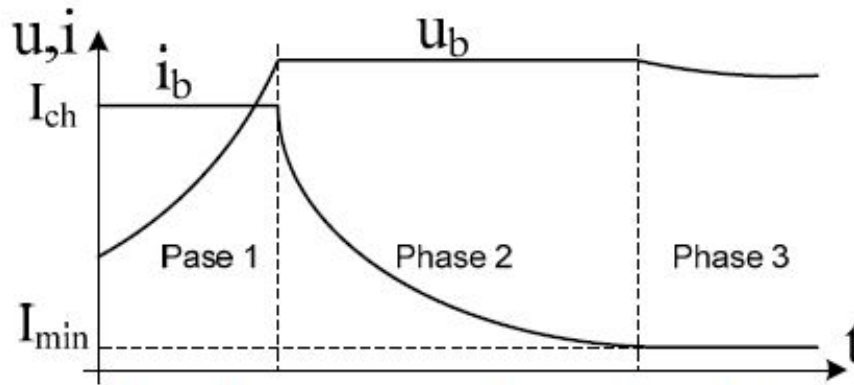


Figure 2.9: Voltage-current characteristic of the inverter interfaced with the battery bank in Reference [21].

2.5.2. BESS Inverter Control

The inverter is responsible for transferring the energy from battery side to MG side and vice versa while matching the MG voltage and frequency. An H-bridge with IGBT or MOSFET and a DC link with a capacitor can accomplish the inverter responsibilities in case of single-phase inverters. The operation of BESS is indispensable to ensure MG operation. Special attention should be paid to BESS inverter control to maintain voltage and frequency stability.

When the microgrid operates in the grid-connected mode, VSIs with current-controlled scheme transfers the power to the microgrid at unity power factor. However, in islanded mode of operation, the VSIs with voltage controlled scheme support the microgrid voltage magnitude and frequency at the PCC [40].

There are mainly two control schemes to be applied on such inverters. The first technique relies on measuring the frequency of the microgrid and controlling the generated active power [14]. The second scheme relies on measuring the generated active power and controlling the microgrid frequency [41].

2.5.3. Battery Power Management

The management of battery power is also a prominent issue besides the microgrid power flow control. Based on cell type (Li-ion, Lead-acid, NiMh,..) there are many conditions to be fulfilled to ensure long battery life. The battery charger exerts a voltage-current characteristic based on the type of the battery. The most well-established method to charge a battery is represented in Figure 2.9. This method is done in three phases: the constant current phase, the constant voltage phase, and the floating phase. In the constant current phase which is also called the bulked phase, the battery bank is charged while the current is constant and the voltage is lower than a predefined set-point. In the constant voltage stage which is also called the absorption stage, the battery bank is discharged while the voltage is constant and the current decreases to reach pre-defined set-point. In the final stage, the battery bank is kept charged by being supplied with a low current. This stage does not reduce the lifetime of the battery by overcharging [21].

The aforementioned strategy to charge the battery bank was adopted from UPS applications in which battery banks are charged completely by the grid voltage and are only utilized emergency cases like black-outs. A UPS system operates rarely, and after every discharge, the grid will charge it thoroughly. However, in an MG a BESS works as an energy buffer, and they will never be charged from start to finish and vice-versa. The reason for such behavior in charging procedure is a result of intermittent nature of RES and demand variation of loads. A solution to the problem of this fluctuation in charging and discharging in BESS is the implementation

of dump loads to dump the battery power fluctuation when there is any surplus of energy production.

2.6. Microgrid Islanding

2.6.1. Local Islanding Detection Techniques

The idea behind the local islanding detection techniques is to monitor the system variables like the voltage and current at the DG side of the PCC to diagnose the islanding when they are out their predefined limits. These local islanding techniques can be categorized under three main methodologies [42].

- Passive techniques.
- Active techniques.
- Hybrid techniques.

Passive Techniques

Passive techniques screen the system parameters such as voltage, frequency, and current on the DG side at the PCC with the main grid. The usual parameters to detect the islanding are frequency and voltage which fluctuate tremendously during the transition between grid connected mode and islanded mode of operation in microgrids. Different passive islanding techniques are as follows [42].

- Under/Over Voltage and Under/Over Frequency: The under/over voltage (UVP/OVP) and under/over frequency (UFP/OFP) are the most aged method to protect distribution networks. The relays are positioned on a feeder in the distribution network and detect the relevant fluctuations in the magnitude and the frequency of the voltage to trip when the range of the variations in the voltage and frequency of the voltage are beyond the corresponding standards [43]. Most of the grid connected PV inverters are using this technique. The protection of such inverters is based on the flow of active and reactive power between PV and the grid at the PCC. The main issue with UVP/OVP and UFP/OFP is the large NDZ [42].

$$\left(\frac{V}{V_{\max}}\right)^2 \leq \frac{\Delta P}{P} \leq \left(\frac{V}{V_{\min}}\right)^2 - 1 \quad (2.11)$$

$$Q_f \left[1 - \left(\frac{f}{f_{\min}}\right)^2\right] \leq \frac{\Delta Q}{P} \leq Q_f \left[1 - \left(\frac{f}{f_{\max}}\right)^2\right] \quad (2.12)$$

Where V_{\min} , V_{\max} , f_{\min} , f_{\max} are the minimum and maximum limits of voltage and frequency, respectively. In Microgrids, P depends on f and Q depends on V [44]. considering the threshold values to be $V_{\min} = 0.8V$ $V_{\max} = 1.2V$ $f_{\min} = 48$ $f_{\max} = 51$ and the $Q_f = 2.5$

$$-30.56\% \leq \frac{\Delta P}{P} \leq 56.25\% \quad (2.13)$$

$$-2.13\% \leq \frac{\Delta Q}{P} \leq 9.71\% \quad (2.14)$$

While active and reactive power variations are within specified limits in islanding mode, the islanding has not been detected. In fact Equations 2.11 and 2.12 define the NDZ for UVP/OVP and UFP/OFP algorithms [44].

- Voltage phase jump detection. Phase jump detection (PJD) screens the sudden leaps of the phase difference between the terminal voltage and output current of the inverter. The PJD method searches for a fast change in the phase to detect whether the microgrid operates in the stand-alone mode of operation or the grid-connected mode of operation. The execution of the method is simple because it requires modifying the same phase locked loop (PLL) that is utilized for synchronizing the DG with the utility grid. The PJD method is not applicable in all operating conditions of the system as it can not detect the islanding mode when the generated power of the DG is equal to the local demand. The none-detected zone (NDZ) in this method is quite smaller than NDZ in (UVP/OVP) and (UFP/OFD) method because PJD detection method is only dependent on the power factor [42]. The PJD algorithm is based on the 2.15 .

$$\arctan\left(\frac{\frac{\Delta Q}{P}}{1 + \frac{\Delta P}{P}}\right) \leq \theta_{\text{threshold}} \quad (2.15)$$

The choice of $\theta_{\text{threshold}}$ must be a trade of between NDZ minization and the effectiveness of detection.

- Harmonic measurement: This method is detecting the islanding mode by measuring selective harmonics (3rd, 5th, etc.) or the total harmonic distortion (THD) of the line voltage and current at the PCC. When the THD is greater than a predefined value the method, diagnose the islanding mode [43].
- Voltage unbalance: The voltage unbalance (VU) is defined as Equation 2.16 where V_2 is the negative sequence and V_1 is the positive sequence of the terminal voltage of the DG. VU technique utilizes the fact that any sudden jump in the load of DG exerts a spike in VU of the DG. A signal is dispatched to the circuit breaker (CB) at the PCC if there is any spike in the value of monitored UV. The downside of this method is the false tripping signal in case of load change at the DG site [45].

$$VU = \frac{V_2}{V_1} \quad (2.16)$$

Active Techniques

The active techniques are mainly used to tackle the problem of NDZ in passive techniques when DG generation matches the load demand perfectly. These methods exert a small signal into the utility grid and monitor the response to detect the islanding. The disturbance is mainly voltage and frequency shift or phase angle shift which could be implemented by the DG. These disturbances in the magnitude and the frequency of the voltage at the PCC will be alleviated by the voltage and frequency control of the utility grid if the microgrid is connected to the utility grid; however, if the voltage and frequency at the PCC track the implemented disturbance that was implemented by DG, the microgrid is probably in the stand-alone mode of operation. The basic idea behind active methods can be depicted in Figure 2.10. The regular methods to implement active detection are as follows [43].

- Active frequency drift (AFD): The AFD method relies on the distortion in the waveform of current which is exerted by using the DG inverter. The inertia of the grid does not allow the voltage at the PCC to fluctuate while the DG is connected to a stiff utility grid. The frequency of the voltage can not change for the similar reason. However, if the DG operates in stand-alone mode and inverter of the DG applies a disturbance on the

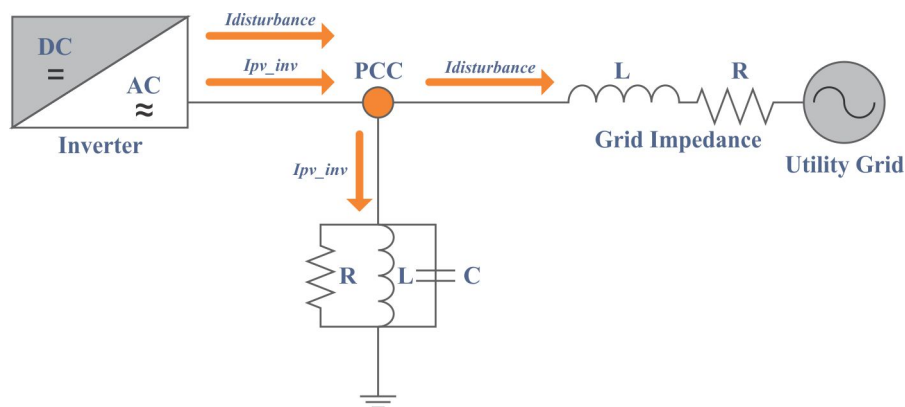


Figure 2.10: A disturbance applied by a PV inverter to the PCC to monitor the islanding

current waveform, the voltage at the PCC will cross zero earlier compared to the time the DG is in grid-connected operation. The frequency should change once again to alleviate the aforementioned jump. This distorted zero crossing changes the phase difference between the voltage and the current at the PCC. The inverter will change the frequency of the current to damp the error in the phase difference. This change in frequency will cause another early zero crossing. This redundant change in the frequency of the voltage at the PCC puts it out the predefined range. A passive method such as UFP/OPF can detect the frequency jump and detect the islanding [46].

- Frequency jump (FJ): FJ applies the methodology of the AFD in a different way. FJ method applies some disturbances into the waveform of output current but not in every cycle. This disturbance can be exerted once in every five cycles. The voltage at the PCC is measured and monitored. The voltage will not get distorted in those specific cycles if the DG is in grid-connected operation. If the DG operates in the stand-alone mode, the distorted waveform will affect the waveform of the voltage, and the islanding can be diagnosed using the same methodology as in AFD [46].
- Impedance measurement: The main principle behind this technique is the same as the one used in passive techniques. A shunt inductance is put in parallel with the DG voltage source. The short circuit current together with the voltage of the voltage source are measured. Dividing the two measured variables would give us the power system impedance. Any change in such a measurement can be used to detect the islanding [46].

3

Microgrid Modeling

3.1. Introduction

In the previous chapter, different levels of control in a microgrid in both stand-alone and grid-connected operation were discussed. Each control level in the hierarchical control structure was discussed, and the level of communication structure needed was mentioned. Battery energy storage systems (BESS) were compared to other means of energy storage in a microgrid and the prominent power electronic interfaces required to implement them in a microgrid were stated. Lastly, an overview of common methods to detect the disconnection of a microgrid from the utility grid with minimum need for ICT was mentioned. In this chapter, a simple microgrid is modeled using the powersys toolbox in Simulink. Each block in the model is discussed, and a brief indication of parameters that were used in each model is given.

3.2. Microgrid Overview

An overview of the microgrid modeled for this thesis is depicted in Figure 3.1. The medium voltage grid is connected through a breaker to the microgrid where the loads are connected to AC side of the microgrid, and the Photovoltaic (PV) panels and BESS are connected to the DC side. A three-phase power electronic converter with six insulated-gate bipolar transistors (IGBTs) connects the AC side to DC side of the microgrid. The three-phase breaker is used to simulate the islanding of the microgrid.

3.3. Battery Energy Storage System Model

The BESS has the most prominent role in the proposed version of the microgrid in this thesis. The battery banks are interfaced through a voltage source converter (VSC) to the rest of the

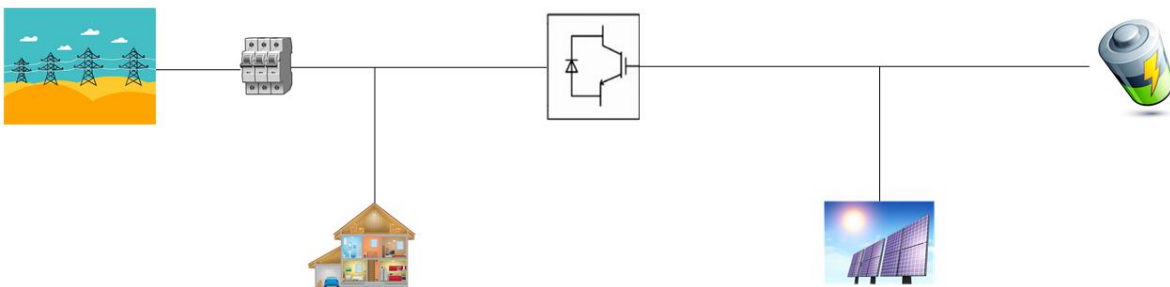


Figure 3.1: An overview of the microgrid modeled in this thesis including the BESS, PV cells, loads, and the grid connection.

microgrid. The BESS should control the state of the charge of the battery (SOC) and support the microgrid by controlling the voltage at the terminal of the VSC when the microgrid is in stand-alone operation.

3.3.1. Battery Model

The battery model block used in this thesis is a parametrized version of a generic model that represents Lithium-Ion batteries. The schematic of the model is represented in the 3.2. The charge and discharge functions are not explained in this thesis; however, a good indication of charge and discharge curves are depicted in Figures 3.3 and 3.4. The discharge curve of the batteries has three main sections. The exponential voltage drop is depicted in the first part while the battery is fully charged. In the second part, the battery can be discharged to the point that the voltage reaches a predefined minimum. In the last section, the total discharge is depicted when the voltage drops with a high slope [47].

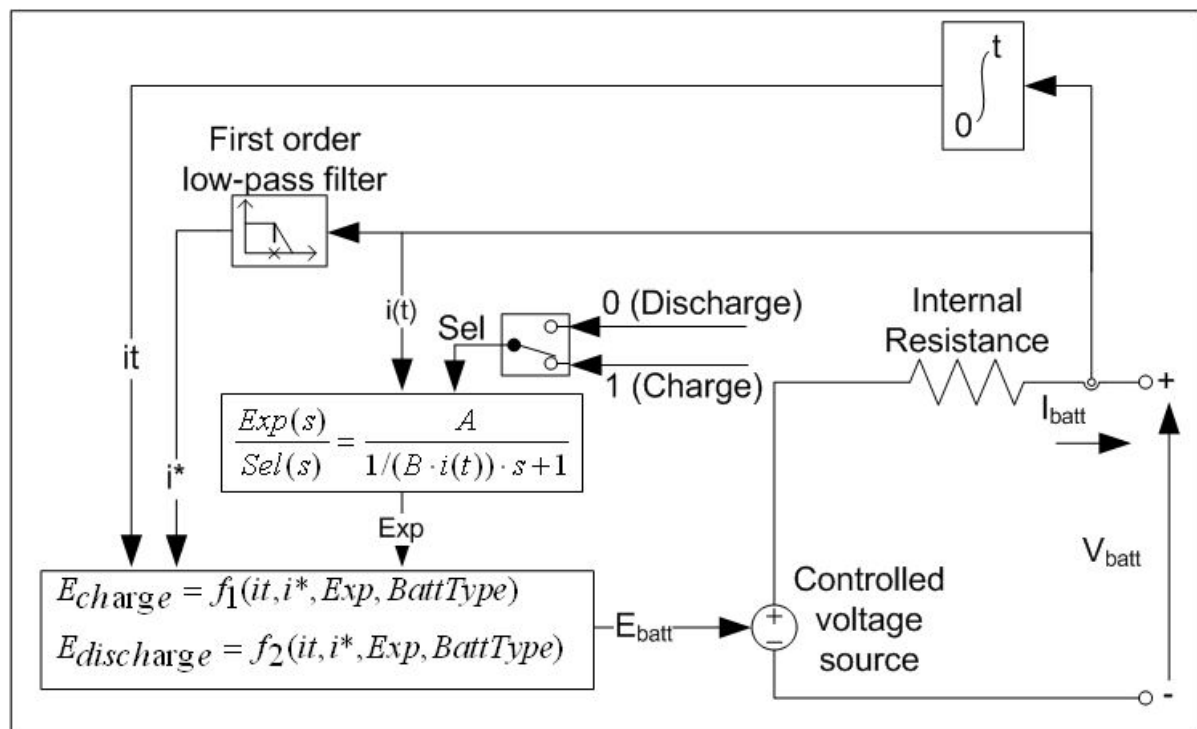


Figure 3.2: Generic battery model of the Li-ion battery modeled in Reference [48].

3.3.2. Voltage Source Converter

The recent advancements in power electronics technology and manufacturing process have increased the switching frequency of Insulated-gate bipolar transistors (IGBTs) drastically. The IGBTs can be switched by controlling the gate voltage, and they don't need any other means of external signals to be turned off. This advantage of IGBTs makes them appropriate candidates to bridge AC and DC networks without a complex switching circuit to like the ones needed for thyristors. The voltage at DC side of the IGBTs is controllable by changing the switching signal at IGBT gates. The voltage at the DC side is stabilized by means of a capacitor [49].

The VSC implemented in this thesis includes six IGBTs, that make a three-phase AC-DC converter. Figure 4.1 represents a three-phase AC to DC converter using IGBTs. The reverse diodes in the IGBTs enable them to flow current in both ways between AC and DC sides. The

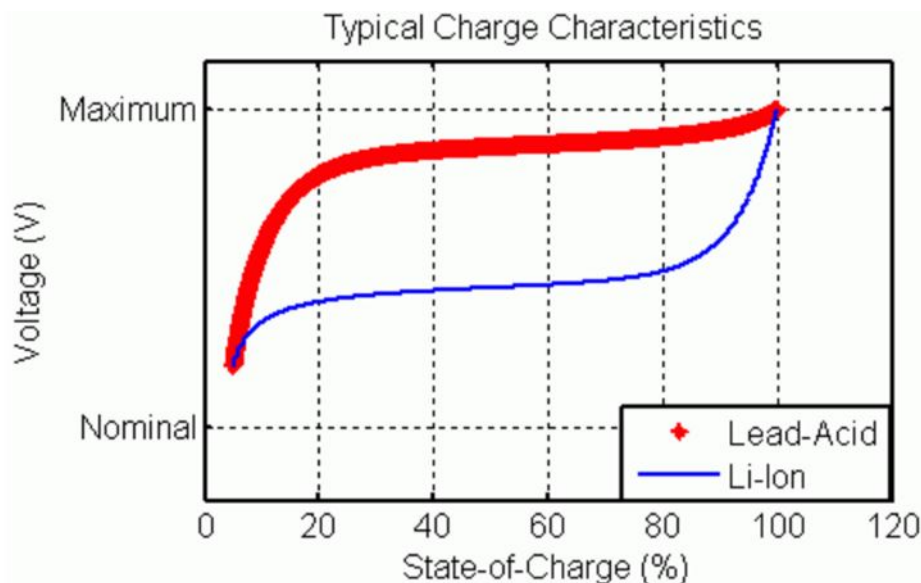


Figure 3.3: Charge characteristic of the Lithium-Ion battery modeled in Reference [48].

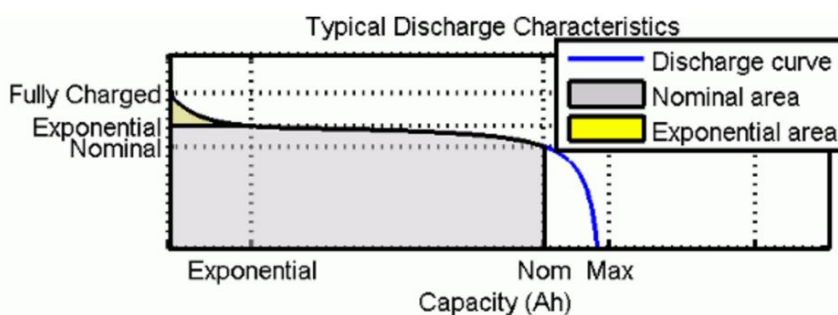


Figure 3.4: discharge characteristic of the Lithium-Ion battery modeled in Reference [48].

VSC can be operated as both a rectifier or an inverter without any change in the topology. However, proper algorithms should be implemented to make it possible. The output power of renewable resources depends on various parameters such as wind speed, irradiation, and temperature. Therefore, unlike conventional resources like gas, oil, and coal the power output of renewables change regularly which is a big challenge from the point of the view of the power system operator. Furthermore, the terminal voltage of solar cells and fuel cells is DC and can not be connected to AC networks directly. The development of VSCs facilitates the integration of renewable sources in a power system. The high degree of freedom in controlling the VSCs allows the solar cells, wind turbines and fuel cells to integrate into power systems using back to back or DC to AC converters. Because of the time-variant nature of the renewable resources, the microgrid requires implementing energy storage to mitigate the uncertainties in power generation and to increase the reliability of the system. Battery and super capacitors are two dominant energy storage systems which are ideal to be implemented in microgrids. Both of them need a VSC to interface with the power system and since the output of the super capacitor and batteries is DC, a DC to AC inverter is necessary to connect them to AC grids. The VSC as a part of BESS is responsible for tracking the active and reactive power set-points. Therefore, a frequency-active power and a voltage-reactive power droop controller could be applied on the VSC to suppress the frequency and voltage deviations following any change in the loads or disconnection from the utility grid. The VSC that is implemented in this thesis has

three arms. Series RC snubber circuits are connected in parallel with each IGBT. A schematic of the VSC is depicted in the Figure 3.5, and The model parameters are listed bellow.

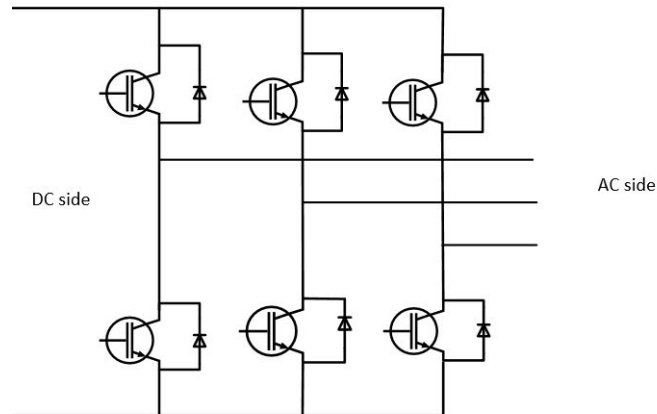


Figure 3.5: Bidirectional VSC with IGBT switches.

- Snubber resistance (R_s) is set to $10 \mu\Omega$.
- Snubber capacitance (C_s) is set to infinity.
- The internal resistance (R_{on}) of IGBTs is set to $1 \text{ m}\Omega$.

3.4. Grid Model

The medium voltage grid is depicted in Figure 3.6 modeled as a three-phase voltage source with following parameters. There is a block implemented between the three-phase voltage source and the transformer which is an ideal voltage and current measurement block.

- Phase-to-phase voltage is 25 kV.
- Frequency is set to 50 Hz.
- Three-phase short-circuit level is 2 MVA.
- $\frac{X}{R}$ is set to 3.

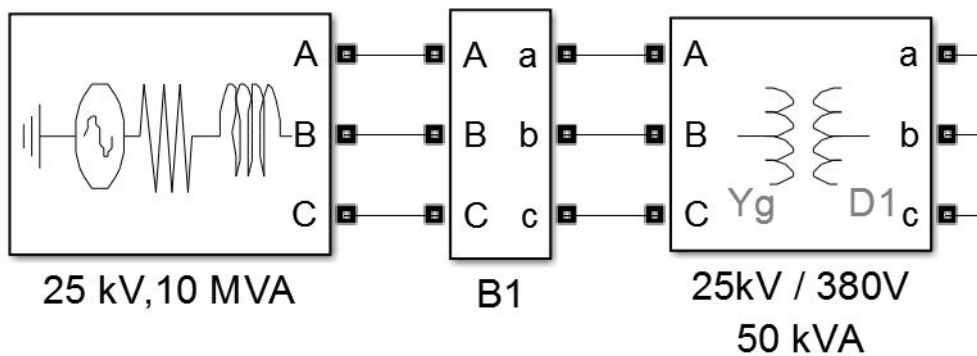


Figure 3.6: Model of the grid together with the voltage and current measurements and the required transformer.

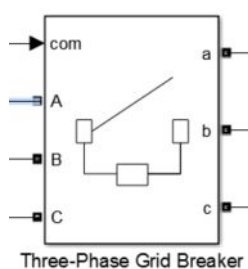


Figure 3.7: Model of the three-phase breaker.

The grid is connected through a two windings three-phase transformer depicted in Figure 3.6 and characterized by the following parameters.

- Primary winding connection is Yg.
- Secondary winding connection Delta(D1).
- Nominal power and frequency is set to 50 kV and 50 Hz.
- Winding 1 voltage(V1) is set to 25 kV.
- Winding 2 voltage(V2) is set to 380 V.
- Resistance and leakage inductance for winding 1 is set to 0.004 PU and 0.02 PU respectively.
- Resistance and leakage inductance for winding 2 are set to 0.004 PU and 0.02 PU respectively.
- Magnetization resistance and inductance is set to 200 PU.

A three-phase breaker is depicted in Figure 3.7 to simulate the islanding behavior of the microgrid. The breaker is put on external switching signal mode to be triggered at certain times to resemble the intentional islanding implementation. The parameters for the Three-phase breaker used in this thesis are as follows.

- Breaker resistance is set to 1 m Ω .
- Snubber resistance is set to 1 $\mu\Omega$.
- Snubber capacitance is set to infinity.

3.5. Cables and Lines

There two main types of cables that should be distinguished in a microgrid model, AC and DC cables. DC cables in a single microgrid cell are short and are used to connect the batteries to the VSC. Therefore, the load impedance of such cables could be ignored. The cables that connect other DERs to either AC or DC side of the microgrid could be AC or DC depending on the type of the DERs. Assuming all the DERs to be located relatively close to the PCC, the corresponding impedance could be ignored. Then, there are the cables than are used to connect the microgrid to the utility grid and the cables that are used to connect the loads to the microgrid. These cables are the ones that their impedances should be modeled since they have a great influence on the modeling of the whole microgrid. If the microgrid cell is

considered to be connected to other microgrid cells as is the case in CSGrid project the cables that are used to connect each microgrid cell to the backbone could be modeled depending on the distance between the microgrid and the backbone.

3.6. Filters

LC filter (resonant filter) used in this model has the following characteristic.

- The inductance of the filter is set to 4 mH.
- The reactive power generated by the filter is set to 8 kvar at 380 V nominal phase-to-phase voltage and 50 Hz nominal frequency.

3.7. Choke

A choke is an inductor to block high-frequency AC signals. In the current model of the microgrid, chokes are modeled as series RL branches. The value for choke parameters is set as follows.

- The resistance of the choke is set to 0.0151 Ω .
- The inductance of the choke is set to 2 mH.

3.8. Load Model

The impact of the loads in a microgrid can not be underestimated when we want to evaluate the overall behavior of the microgrid. For example, when a motor is connected to a grid without any power electronic interface in between, it is coupled directly to the grid and adds an inertia. This inertia does not allow the frequency deviations to happen instantaneously. The motor should increase or decrease its acceleration by injecting to or consuming power from the grid. Contrary to the rotating loads like motors, a light bulb does not have any frequency effect on the microgrid, and it will act just like a constant impedance. Therefore, load modeling is not an easy task due to different types of loads that could be found in a microgrid. Even if the characteristics of all available loads in a microgrid is understood modeling them all would be a time-consuming task. Exploring the load behavior in a microgrid is out of the scope of this thesis. Thus a simple load model is exerted. There are two broad type of loads that could be modeled in a microgrid, static or dynamic loads. Static loads are characterized by constant power, constant current and constant impedance. The static load is used for modeling the sample loads in this thesis, and the constant power type is chosen. The loads are modeled as series RLCs. The loads are used to connect and disconnect from the microgrid to evaluate the voltage and frequency response of the control strategy implemented on the voltage source converter. The values for the load parameters are as following.

- Active power consumption of each load is 100 kW.
- Reactive power consumption of each load is 50 kvar.
- Three-phase line-to-line voltage is 380 V.

3.9. PV Model

The intermittent nature of the solar irradiation makes it an uncontrollable source meaning there is no guarantee that the excess power needed when the microgrid is disconnected from

the utility grid, can be supplied from the PV panels. Thus, the support from PV panels can not be relied on, during the transition of the microgrid from the grid connected mode to the stand-alone mode of operation. The support is solely provided by the BESS during the transition between two modes of operation of the microgrid, and the inverter control of PV panels is less important than the one being implemented on battery banks. Therefore, the PV panels could be modeled as a generic dynamic load with negative parameters which produce active and reactive power instead of consuming them. The PV panels together with the DC to AC inverter could be modeled as the dynamic load with following parameters.

- Nominal line to line voltage is set at the inverter side is set to 380 V.
- Active and reactive power at initial voltage are set to 100 kW.

3.10. Measurement Process

3.10.1. DQ Transformation

The dq0 transformation which is also called Park transformation is a vector space transformation of three-phase time-domain signals from a stationary phase coordinate system (ABC) to a rotating coordinate system (dq0). The dq0 transform is essentially an extension of the Clarke transformation, which applies an enable transformation to convert from stationary reference frame to a synchronously rotating frame. The synchronous reference frame can be aligned to rotate with the voltage as is used in voltage source converters or with the current as is used in current sourced converters [50]. In this thesis; the dq0 transformation is applied to obtain the mathematical model for the microgrid. The advantage of using the dq0 transformation is to remove the time-variant coefficients. The transformation matrix and the inverse transformation matrix are defined as follows:

$$A = \begin{bmatrix} \cos(\theta) & -\sin(\theta) & 1 \\ \cos(\theta - \frac{2\pi}{3}) & -\sin(\theta - \frac{2\pi}{3}) & 1 \\ \cos(\theta + \frac{2\pi}{3}) & -\sin(\theta + \frac{2\pi}{3}) & 1 \end{bmatrix}$$

(3.1)

$$A^{-1} = \frac{2}{3} \begin{bmatrix} \cos(\theta) & \cos(\theta - \frac{2\pi}{3}) & \cos(\theta + \frac{2\pi}{3}) \\ -\sin(\theta) & -\sin(\theta - \frac{2\pi}{3}) & -\sin(\theta + \frac{2\pi}{3}) \\ \frac{1}{2} & \frac{1}{2} & \frac{1}{2} \end{bmatrix}$$

(3.2)

where $\theta = \Omega t + \delta_a$ is the angle between the rotating and fixed coordinate system and each time t and a is the initial phase shift of the voltage. The graphical representation of the corresponding vectors is depicted in Figure 3.8. Interestingly, the zero component in the dq0 transformation is the same as the zero component in the symmetrical components transform. For example the zero sequence component of the voltage is $\frac{1}{3}(V_a + V_b + V_c)$ in both dq0 transformation and symmetrical components transformation.

The relation between the variables in the abc frame(in this case the terminal voltage) and the new variables in dq0 frame are thus:

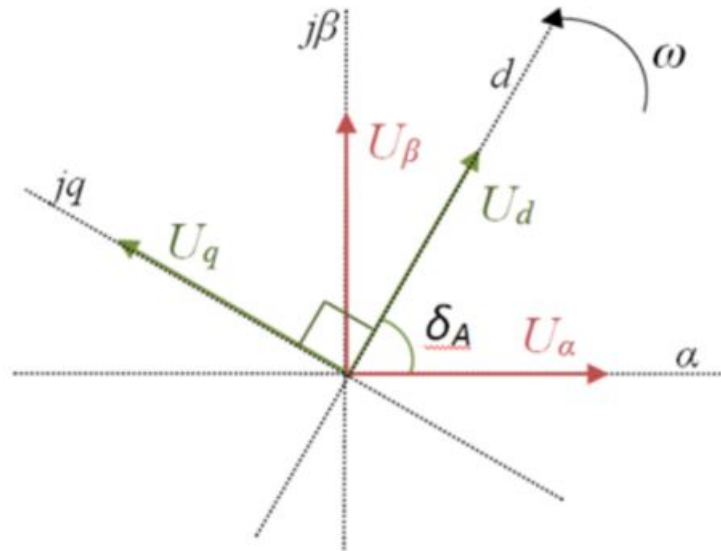


Figure 3.8: dq0 transformation [51].

$$V_{dq0} = A.V_{abc} \quad (3.3)$$

$$V_{abc} = A^{-1}.V_{dq0} \quad (3.4)$$

Where,

$$V_{abc} = \begin{bmatrix} V_a \\ V_b \\ V_c \end{bmatrix}, V_{dq0} = \begin{bmatrix} V_d \\ V_q \\ V_0 \end{bmatrix} \quad (3.5)$$

3.10.2. The Application of dq0 Transformation on a Balanced Three Phase Voltage

The following equations take a two-phase quadrature voltage along the stationary frame and transform it into a two-phase synchronous frame. In the dq0 frame, the zero component is the same as the one in $\alpha\beta 0$. frame.

3.10.3. Instantaneous Power in dq0 Frame

The instantaneous active and reactive power can be derived as follows.

$$p = V_d I_d + V_q I_q \quad (3.6)$$

$$q = V_q I_d - V_d I_q \quad (3.7)$$

When the synchronous frame is aligned to voltage the quadrature component is zero and the equations could be simplified as bellow.

$$p = V_d I_d \quad (3.8)$$

$$q = -V_d I_q \quad (3.9)$$

These equations show that the independent control of active and reactive power is possible using the dq0 transformation of current components. (I_d and I_q).

3.10.4. Time Invariant Version of dq0 Transformation

The classical dq0 transformation is power variant. It means that the instantaneous power of the variables calculated in the dq0 frame is not the same as the active and reactive power calculated in the abc frame. A power invariant version of the dq0 transformation is defined as follows:

$$\begin{bmatrix} V_d \\ V_q \\ V_0 \end{bmatrix} = \sqrt{\frac{2}{3}} \begin{bmatrix} \cos(\theta) & \cos(\theta - \frac{2\pi}{3}) & \cos(\theta + \frac{2\pi}{3}) \\ -\sin(\theta) & -\sin(\theta - \frac{2\pi}{3}) & -\sin(\theta + \frac{2\pi}{3}) \\ \frac{1}{\sqrt{2}} & \frac{1}{\sqrt{2}} & \frac{1}{\sqrt{2}} \end{bmatrix} \begin{bmatrix} V_a \\ V_b \\ V_0 \end{bmatrix}$$

$$\begin{bmatrix} V_a \\ V_b \\ V_0 \end{bmatrix} = \sqrt{\frac{2}{3}} \begin{bmatrix} \cos(\theta) & -\sin(\theta) & \frac{\sqrt{2}}{2} \\ \cos(\theta - \frac{2\pi}{3}) & -\sin(\theta - \frac{2\pi}{3}) & \frac{\sqrt{2}}{2} \\ \cos(\theta + \frac{2\pi}{3}) & -\sin(\theta + \frac{2\pi}{3}) & \frac{\sqrt{2}}{2} \end{bmatrix} \begin{bmatrix} V_d \\ V_q \\ V_0 \end{bmatrix}$$

(3.11)

4

Control strategy

4.1. Introduction

In the previous chapter, a microgrid was parameterized to be used as a base model for the evaluation of the control strategies which are going to be proposed in this chapter. The main objective of this chapter to propose some control schemes which can be implemented in BESS to enable the microgrid to have a stable operation in grid-connected and stand-alone modes of the operation. The implemented control scheme should also guarantee a smooth transition between the two operation modes. Different case studies will be implemented in this chapter to demonstrate the real-world case scenarios. A dual-control strategy is defined, and the effectiveness of the controller is evaluated through various case studies. The results of the simulations will be depicted in the next chapter.

4.2. Case Studies

Three main case studies should be taken into account in this chapter to emulate the operation of the controllers applied on the connected VSC to the battery banks. For each case study, a control strategy is proposed. Therefore, three main control modes are discussed in this chapter: the current controlled mode which is also called power control mode, voltage/frequency control mode, and dual-control mode which is used to tackle the problem during the transition between two modes of operation in a microgrid. The three case studies which are discussed in this chapter are as following:

- Grid-connected case study.
- Stand-alone case study.
- Transition mode case study.

4.2.1. Grid-connected Mode Control Strategy

The two-level VSC that was proposed in chapter 3 is repeated here in Figure 4.1 for ease of reference. The converter is called a two-level VSC because the output AC voltage of each phase can toggle between two levels.

For a microgrid operating in grid-connected mode, VSCs that are interfaced with batteries can operate in current-controlled mode. Based on the SOC of the batteries, and active power requirements by the microgrid, the battery bank is being charged or discharged at any given moment. The BESS participates in regulating power flow and not the system frequency when

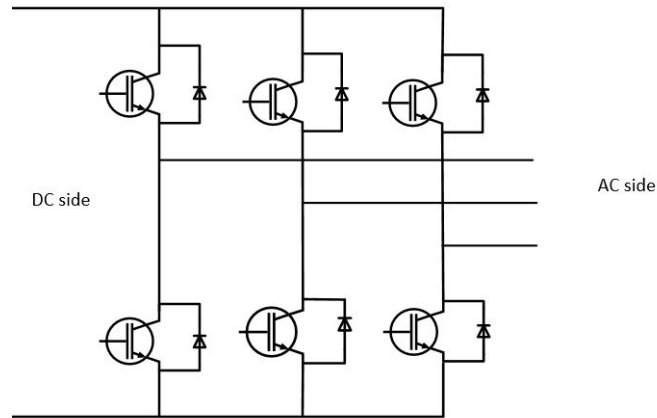


Figure 4.1: Bidirectional VSC with IGBT switches.

the microgrid is connected to the utility grid, so this control strategy is also called the power control strategy. The power control mode has mainly two loop controls: inner current control loop and outer power control loop. For the implementation of the control strategy a decoupled dq transformation is used which was presented in Figure 3.10.4. Variables in the abc system are transformed into the synchronous reference frame. In this chapter, we consider the microgrid to be connected to an infinitely stiff grid when it is in grid-connected mode. Therefore, the AC power system is modeled as an ideal three-phase voltage source. The battery model, which is used in the simulation of the microgrid, has operational limits. However, for implementing the control strategies, the battery model is simplified in this chapter and modeled as an ideal DC voltage source.

Before building up a battery controller for the microgrid proposed in chapter 3, a controller is proposed for an ideal dc voltage source which is connected through a two-level VSC to an AC source. The equivalent model for such a circuit is depicted in Figure 4.2.

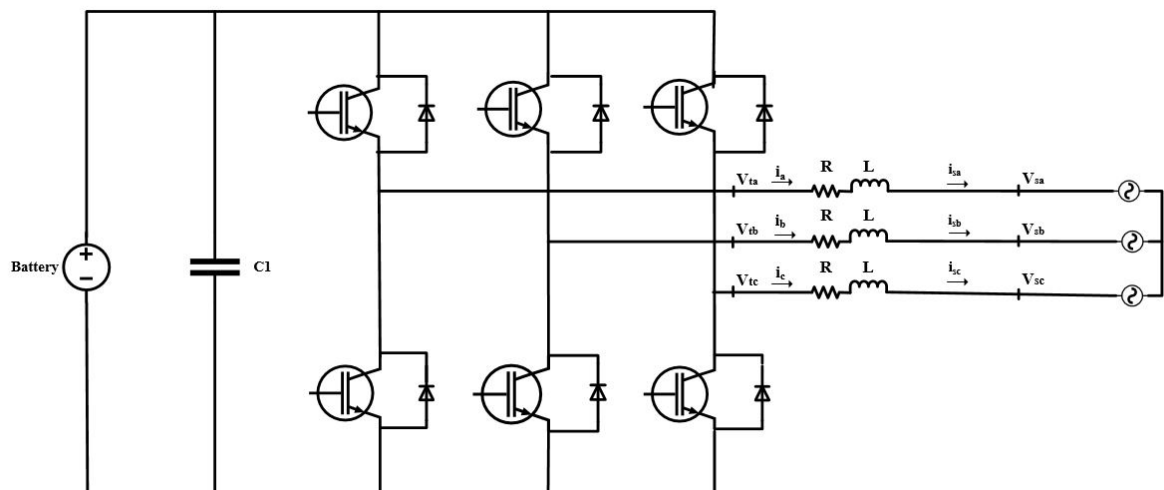


Figure 4.2: An ideal DC source as a simple model for a battery connected to an AC source through a two level VSC.

The AC voltages at the AC source are expressed as:

$$\begin{aligned}
 V_{sa}(t) &= \hat{V}_s \cos(\omega t + \theta_0) \\
 V_{sb}(t) &= \hat{V}_s \cos(\omega t + \theta_0 - \frac{2\pi}{3}) \\
 V_{sc}(t) &= \hat{V}_s \cos(\omega t + \theta_0 - \frac{4\pi}{3})
 \end{aligned}
 \tag{4.1}$$

where ω is the angular frequency of the AC source, \hat{V}_s is the peak line to neutral voltage and θ_0 is the initial phase angle of the source.

The dynamic of AC side of the circuit could be described as follows.

$$\begin{aligned}
 L \frac{di_a}{dt} &= -Ri_a + V_{ta} - V_{sa} \\
 L \frac{di_b}{dt} &= -Ri_b + V_{tb} - V_{sb} \\
 L \frac{di_c}{dt} &= -Ri_c + V_{tc} - V_{sc}
 \end{aligned}
 \tag{4.2}$$

where R and L are the series resistance and inductance by which each phase of the VSC is interfaced with the AC system. Variables in the abc system can be transformed into the dq system (synchronous reference frame) using transformation matrix in Equation 3.10.4. The terms in Equation 4.2 can be rewritten as following:

$$\begin{aligned}
 L \frac{di_d}{dt} &= -Ri_d + L\omega(t)i_d + V_{td} - V_{sd} \\
 L \frac{di_q}{dt} &= -Ri_q - L\omega(t)i_q + V_{tq} - V_{sq}
 \end{aligned}
 \tag{4.3}$$

The power exchanged at the PCC could be derived as follows

$$\begin{aligned}
 P(t) &= \frac{3}{2} [V_{sd}i_d + V_{sq}i_q] \\
 Q(t) &= \frac{3}{2} [-V_{sd}i_q + V_{sq}i_d]
 \end{aligned}
 \tag{4.4}$$

Now is the time to introduce a new control variable ρ where $\omega = \frac{d\rho}{dt}$ and

$$\begin{aligned} V_{sd} &= \hat{V}_s \cos(\omega_0 t + \theta_0 - \rho) \\ V_{sq} &= \hat{V}_s \sin(\omega_0 t + \theta_0 - \rho) \end{aligned} \quad (4.5)$$

V_{sd} and V_{sq} are the voltage components of the AC source in the synchronous frame. In the equations above i_d and i_q , and ρ are the state variables and V_{td} , V_{tq} , and ω are the control variables. if $\rho(t) = \omega_0(t) + \theta_0$ then the $V_{sq} = 0$. Keeping V_{sq} at zero using a phased locked loop (PLL) the power exchanged with the AC source at the PCC can be rewritten as:

$$\begin{aligned} P(t) &= \frac{3}{2} V_{sd} i_d \\ Q(t) &= -\frac{3}{2} V_{sd} i_q \end{aligned} \quad (4.6)$$

As V_{sd} is constant, the active and reactive power at the PCC can be controlled by i_d and i_q . Now it is time to define the reference values for i_d and i_q as

$$\begin{aligned} i_{dref}(t) &= \frac{2}{3V_{sd}} P_{sref}(t) \\ i_{qref}(t) &= -\frac{2}{3V_{sd}} Q_{sref}(t) \end{aligned}$$

Therefore, if a fast controller is applied on the VSC in such a way that $i_d = i_{dref}$ and $i_q = i_{qref}$, then $P_s = P_{sref}$ and $Q_s = Q_{sref}$, and therefore P_s and Q_s can be controlled independently by their reference values. It is worth mentioning that as i_{dref} , i_{qref} , and V_{sd} are in steady state, By choosing P_{sref} and Q_{sref} as constant signals, the control of the sinusoidal abc variables has been modeled as the control of DC variables in synchronous frame. The problem of controlling active and reactive power which is exchanged between the VSC and AC voltage source at the PCC is simplified to controlling i_d and i_q .

Control of i_d and i_q

From Equation 4.3 and the assumption of being in steady-state by substituting ω_0 into $\omega(t)$, we have:

Also, the VSC terminal voltages in dq frame can be calculated by:

where $m_d(t)$ and $m_q(t)$ are the dq components of $m(t)$ (modulating signal) which are used to control pulse-width modulation (PWM) switching [52]. The Equation 4.2.1 describe the VSC model in the dq frame. The presence of the $L\omega_0$ terms makes the dynamic behavior of i_d and i_q to be coupled together. To make them decoupled the m_d and m_q can be determined as where u_d and u_q are two new control signals [53], [54]. Reformulating Equation 4.2.1 by substituting V_{td} and V_{qd} from 4.2.1 and substituting m_d and m_q from 4.2.1 we have:

Equation 4.2.1 describe two linear systems which are decoupled. These two equations also show that i_d and i_q are controllable by means of u_d and u_q . Figure 4.3 shows the representation of the current controllers applied on the VSC proposed in Figure 4.2. The d-axis compensator processes $e_d = i_{dref} - i_d$ and produces the control signal u_d . Based on 4.2.1,

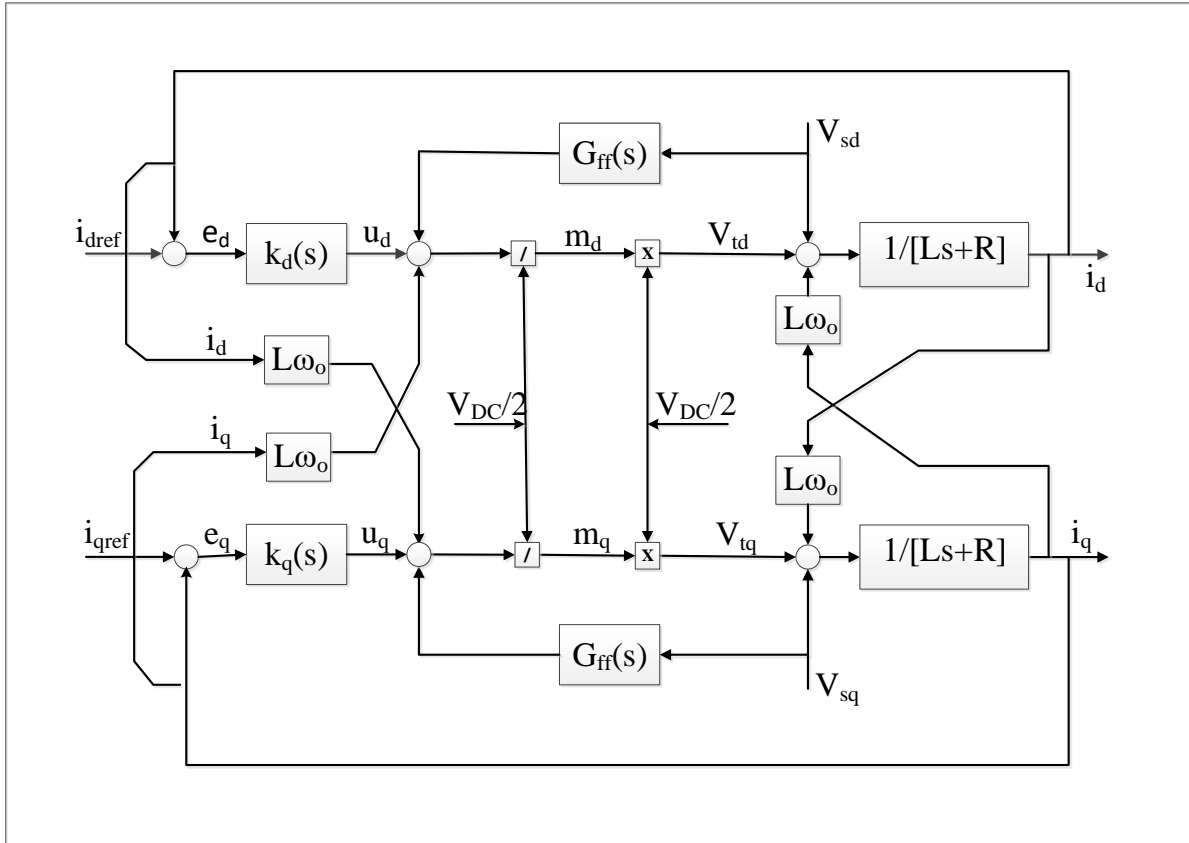


Figure 4.3: The control scheme implemented on the VSC when it is connecting a battery to an AC source.

m_d signal is produced. A similar approach is used to compensate e_q . u_q is the output signal of the corresponding compensator and m_q is calculated by Equation 4.2.1. The VSC generates V_{td} and V_{tq} by multiplying m_d and m_q by $\frac{V_{DC}}{2}$. Based on the control process in Figure 4.3, a simplified control block can be extracted and is depicted in Figure 4.4.

Figure 4.4 shows that the control plants in the d-axis and q-axis current control loop are similar. Therefore, the corresponding compensators can also be identical. In the d-axis control loop, a proportional-integral (PI) compensator is capable of tracking i_{dref} as a DC reference. Therefore, let's define K_d as $\frac{k_p s + k_i}{s}$. The k_p and k_i are proportional and integral gains. Thus the loop gain is:

$$\ell(s) = \frac{k_p}{Ls} \times \left(\frac{s + \frac{k_i}{k_p}}{s + \frac{R}{L}} \right) \quad (4.8)$$

The plant pole at $s = \frac{R}{L}$ is close to the origin and causes the magnitude, and the phase of the loop gain to drop at low frequencies. Therefore, the plant pole is first cancelled by the compensator zero $s = \frac{k_i}{k_p}$ and loop gain gets the form of $\ell(s) = \frac{k_p}{Ls}$. Thus, the closed loop transfer function is:

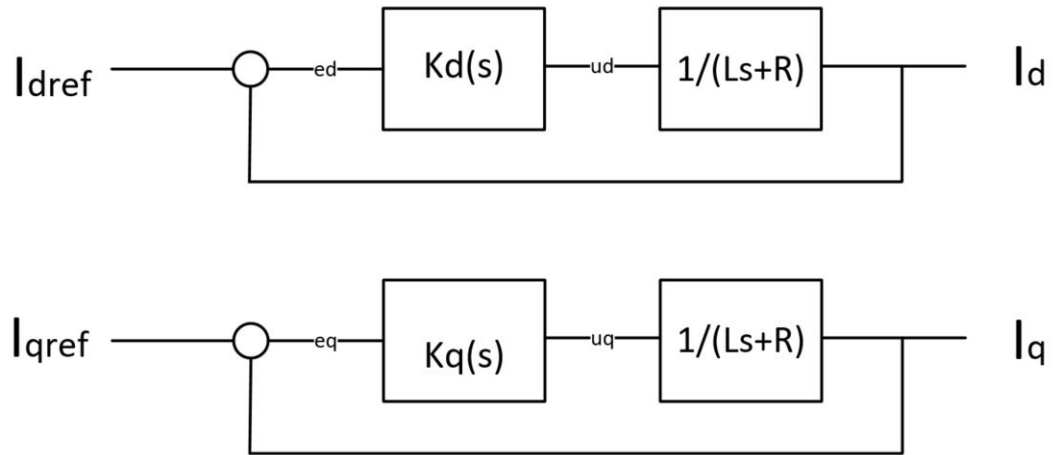


Figure 4.4: The simplified control blocks implemented on the VSC when it is connecting a battery modeled by DC source to an AC source.

$$\begin{aligned}
 G_i(s) &= \frac{I_d}{I_{dref}(s)} \\
 &= \frac{L(s)}{1 + L(s)} \\
 &= \frac{1}{\tau s + 1}
 \end{aligned} \tag{4.9}$$

where

$$\begin{aligned}
 k_p &= \frac{L}{\tau_i} \\
 k_i &= \frac{R}{\tau_i}
 \end{aligned} \tag{4.10}$$

in which, τ_i is the time constant of the closed loop and is a design choice. τ_i has to be small to have a fast control response but sufficiently large to have a small bandwidth of the closed-loop control systems compared to the switching frequency of the VSC. Depending on the application for which the controller is designed, τ_i is selected in the range of 0.5 to 5 ms [55]. The identical control loops for i_d and i_q suggest to use the same values for design of the $k_q(s)$.

4.2.2. Stand-alone Mode of The Operation

In the previous section, the control blocks were designed to control a VSC when the microgrid is connected to the utility grid. In this section, the control of a VSC is investigated when the microgrid is switched to the stand-alone mode. The operating frequency is not imposed by utility grid anymore, so the VSC controller maintain the frequency at the PCC. The VSC in this BESS is thus, a controlled-frequency VSC. The active and reactive power are not controlled by the VSC controller opposed to the case when the microgrid was connected to the grid.

In the new BESS, the VSC terminal is interfaced with the three phase load via an RLC filter as depicted in Figure 4.5. The filter is made of an RL series branch and a shunt C_f . C_f provides

a steady voltage at the node connected to the RL series branch. The current controlled VSC produces the active and reactive power (P_s, Q_s) and C_f produces Q_c . Therefore, the active and reactive power which are fed into the load is P_s and $Q_s + Q_c$ respectively. From the current-controlled VSC, if we substitute V_s by V_L , the Laplace form of the compensators can be written as:

$$K_d(s) = K_q(s) = \frac{k_p s + k_i}{s} \quad (4.11)$$

Therefore, the Laplace form of the i_d and i_q signals can be written as:

$$\begin{aligned} I_d(s) &= G_i(s)I_{dref}(s) = \frac{1}{\tau s + a} I_{dref}(s) \\ I_q(s) &= G_i(s)I_{qref}(s) = \frac{1}{\tau s + a} I_{qref}(s) \end{aligned} \quad (4.12)$$

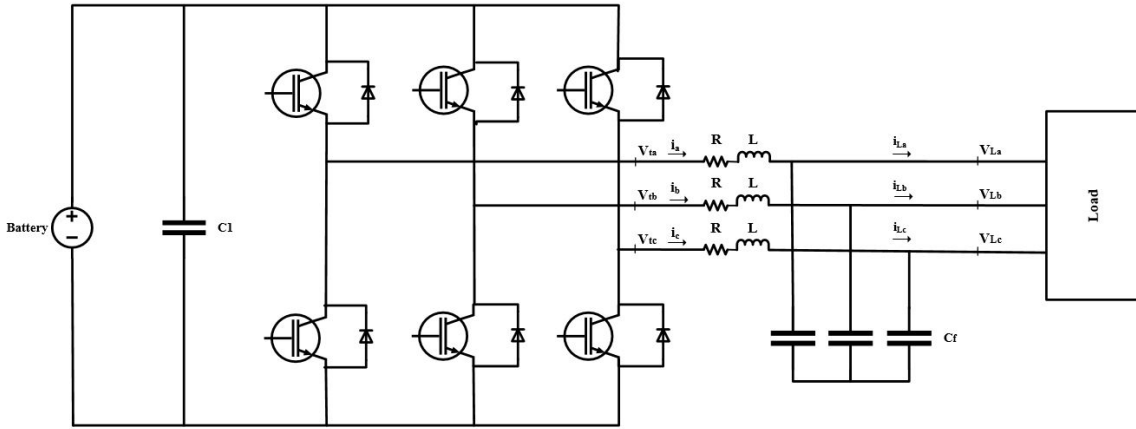


Figure 4.5: VSC system when it is connecting a battery as a DC source to a three phase load.

Based on Figure 4.5 the dynamic equations of the load voltages can be written as:

$$\begin{aligned} C_f \frac{dV_{La}}{dt} &= i_a - i_{La} \\ C_f \frac{dV_{Lb}}{dt} &= i_b - i_{Lb} \\ C_f \frac{dV_{Lc}}{dt} &= i_c - i_{Lc} \end{aligned} \quad (4.13)$$

Transforming Equation 4.13 from abc frame to dq frame, we have:

$$\begin{aligned} C_f \frac{dV_{Ld}}{dt} &= C_f \omega V_{Lq} + i_d - i_{Ld} \\ C_f \frac{dV_{Lq}}{dt} &= -C_f \omega V_{Ld} + i_q - i_{Lq} \end{aligned} \quad (4.14)$$

The control objective is to regulate the frequency and the magnitude of load voltage (\hat{V}_L). Keeping the value of the load voltage at a certain level of nominal voltage (V_n) means that

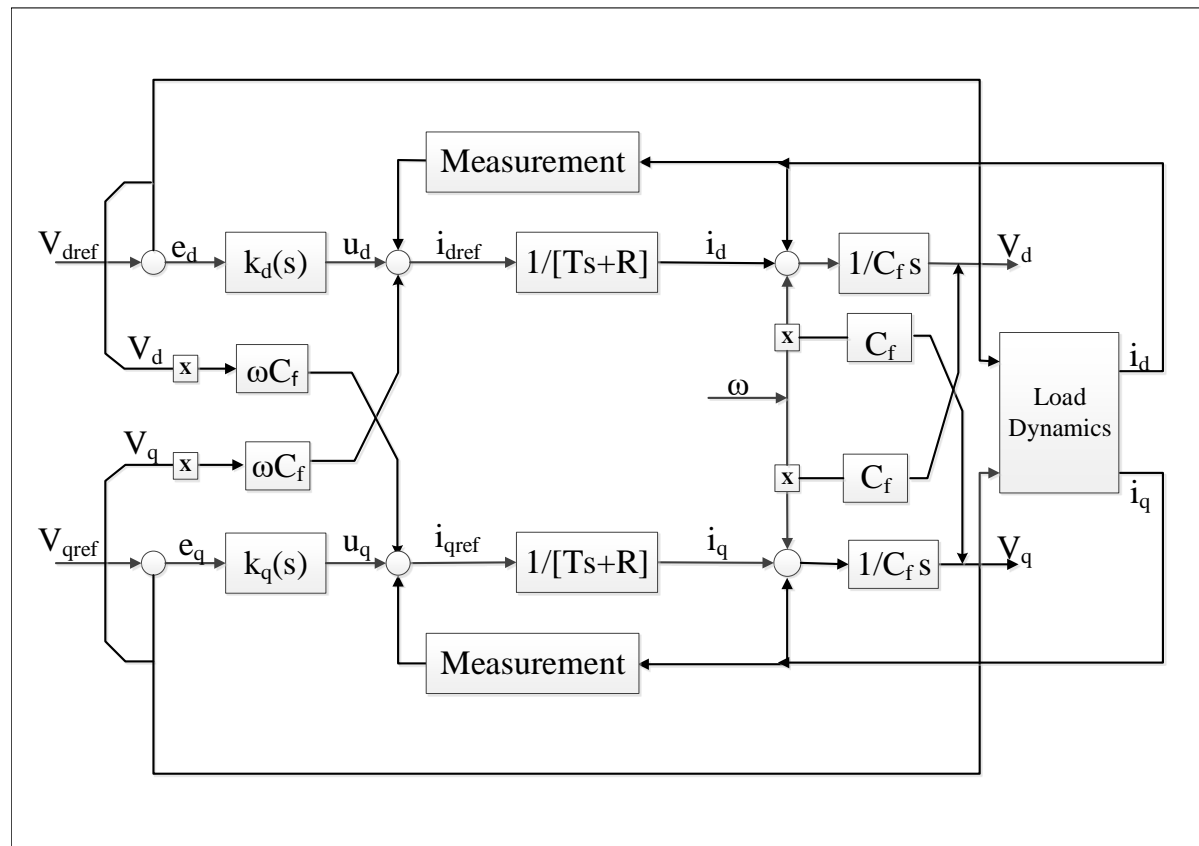


Figure 4.6: Control scheme implemented on a VSC system when it is connecting a battery modeled as a DC source to a three phase load.

the tip of the vector of V_L would be on the contour of a circle with the radius of V_n . On the other hand, $V_L = \sqrt{(V_{Ld})^2 + (V_{Lq})^2}$ gives us the possibility to choose V_{Ld} as V_n and V_{Lq} as 0. This idea is the same idea we implemented in current-controlled VSC controller in which the V_{sq} was kept at zero level by using a PLL. Investigating the dynamic models of different loads reveals the fact that V_{Ld} and V_{Lq} are extremely inter-coupled even for a simple RL load [55]. Therefore, the design of a controller which guarantees the closed-loop stability is not an easy task. To resolve this complexity, a feed-forward compensation is used to eliminate the coupling between V_{Ld} and V_{Lq} [56].

The feedforward compensation signal is like the one that was used to decouple i_d and i_q in the current-controlled VSC proposed for the grid-connected operation of the microgrid. This decoupling method provides the possibility for controlling V_{Ld} by i_{dref} , and V_{Lq} by i_{qref} . Based on Figure 4.6, the i_{dref} and i_{qref} are expressed by:

$$\begin{aligned} i_{dref} &= u_d - C_f(\omega V_{Lq}) + i_{Ld} \\ i_{qref} &= u_q + C_f(\omega V_{Ld}) + i_{Lq} \end{aligned} \quad (4.15)$$

u_d and u_q are defined as two new control signals the same way they were formulated for the grid-connected operation of the VSC. Rewriting the Equation 4.12 by substituting i_{dref} and i_{qref} the new Laplace form of i_d and i_q are derived as

$$\begin{aligned} I_d(s) &= G_i(s)U_d(s) - C_f G_i(s)\mathcal{L}(\omega V_{sq}) + G_i(s)I_{Ld}(s) \\ I_q(s) &= G_i(s)U_q(s) + C_f G_i(s)\mathcal{L}(\omega V_{sd}) + G_i(s)I_{Lq}(s) \end{aligned} \quad (4.16)$$

Applying the Laplace operator on Equation 4.14, and substituting $I_d(s)$ and $I_q(s)$ from Equation 4.16 we have:

$$\begin{aligned} C_f s V_{Ld}(s) &= G_i(s) U_d(s) + C_f [1 - G_i(s)] \mathcal{L}(\omega V_{sq}) - [1 - G_i(s)] I_{Ld}(s) \\ C_f s V_{Lq}(s) &= G_i(s) U_q(s) - C_f [1 - G_i(s)] \mathcal{L}(\omega V_{sd}) - [1 - G_i(s)] I_{Lq}(s) \end{aligned} \quad (4.17)$$

where $G_i(s)$ is $\frac{1}{\tau_i s + 1}$ and has a unity DC gain, and therefore the term $1 - G_i(s) = \frac{\tau_i s}{1 + \tau_i s + 1}$ has no DC gain. For small τ , $1 - G_i(s)$ can be neglected over the wide range of frequencies. This simplification will help to rewrite the Equation 4.17 as:

$$\begin{aligned} \frac{V_{Ld}(s)}{U_d(s)} &= G_i(s) \frac{1}{C_f s} \\ \frac{V_{Lq}(s)}{U_q(s)} &= G_i(s) \frac{1}{C_f s} \end{aligned} \quad (4.18)$$

The above equations show two systems in which u_d and u_q are the inputs and V_{Ld} and V_{Lq} are the outputs. These two systems are decoupled and V_{Ld} and V_{Lq} can be controlled independently.

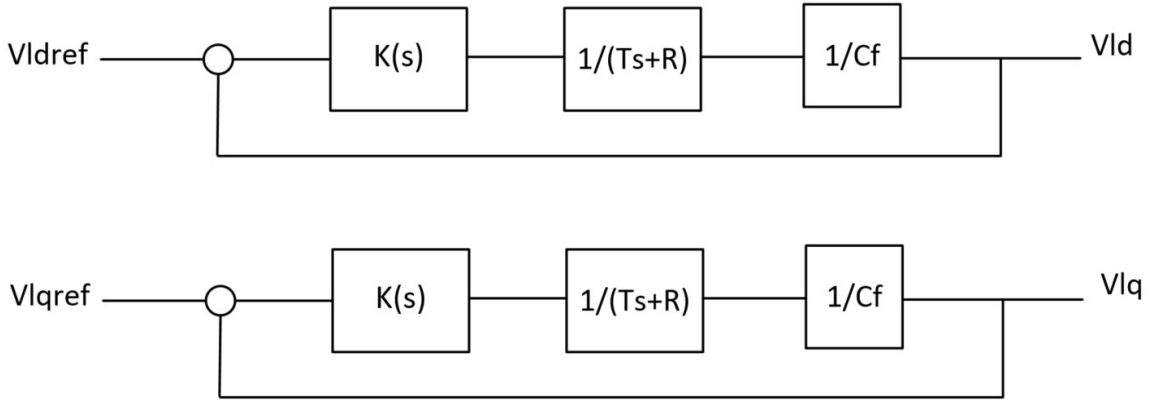


Figure 4.7: The control scheme implemented on the VSC when it is connecting a DC source to an AC source.

It can be seen from Figure 4.6 that u_d and u_q are the result of two decoupled compensators. The first compensator deals with e_d and the second one deals with e_q producing u_d and u_q respectively. i_{dref} and i_{qref} are derived by 4.15 and are injected into the corresponding current control loops in dq axis. The block diagram of Figure 4.6 can thus be simplified as the block diagram represented in Figure 4.7. Each control loop in this Figure has a integral term and a real pole at $s = -\frac{1}{\tau}$. The simplest approach to design such a system is to implement a PI compensator. Such a compensator could be described by

$$k(s) = k \frac{s + z}{s} \quad (4.19)$$

Thus the closed loop gain is expressed by:

$$\ell(s) = \frac{k}{\tau C_f} \left(\frac{s + z}{s + \frac{1}{\tau}} \right) \frac{1}{s^2} \quad (4.20)$$

and δ_m as the maximum phase of $\ell(j\omega)$ and ω_m the corresponding angular frequency can be calculated by

$$\delta_m = \arcsin\left(\frac{1 - \tau z}{1 + \tau z}\right) \quad (4.21)$$

$$\omega_m = \sqrt{\frac{z}{\tau}}$$

4.2.3. Transition Mode of Operation

In the previous sections, two separate control methods were proposed for a battery system in two different modes of operation. As discussed in Chapter 2, due to different circumstances such as maintenance requirements or a fault in the utility grid, the microgrid is required to switch between grid connected mode and stand-alone mode of operation. The process in which a microgrid is switched from grid connected mode to stand-alone mode is called islanding and the process in which microgrid is switched from stand-alone mode to grid connected mode is called de-islanding. For the investigation of the transition between these two modes, a new microgrid topology is defined and depicted in Figure 4.8.

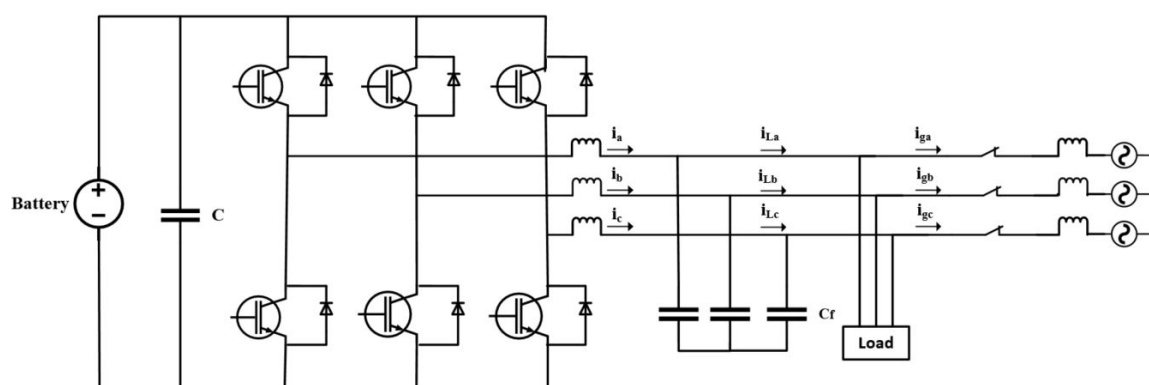


Figure 4.8: The topology of the VSC system when it is connecting a battery to an AC source with the presence of the breaker to simulate the islanding.

In this Figure, the current controlled BESS is connected through a breaker to the grid. The breaker in this model is used to simulate the islanding operation and resynchronization process. PCC is the point at which VSC terminals, load terminals, and grid lines are connected to each other. When the switch is closed, the load voltage V_{Labc} is equal to V_{gabc} and forced by the grid. In this operation mode, the VSC system behaves as an active-reactive power controller. Therefore, the power which is delivered to the grid side would be power out of the VSC terminals minus the power which is consumed by the load. The active and reactive power produced by VSC system is thus controllable by i_{dref} and i_{qref} as discussed in section 4.2.1. If the breaker opens as a result of a maintenance operation or a fault at the grid side, the system consisting of BESS and load is isolated from the grid. In this new operation mode, the VSC control should also switch from the frequency imposed operation to the frequency/voltage control operation to keep the voltage and frequency at their corresponding nominal values. In the new operation mode, i_{dref} and i_{qref} should be calculated based on the voltage regulation

method that was proposed in section 4.2.2.

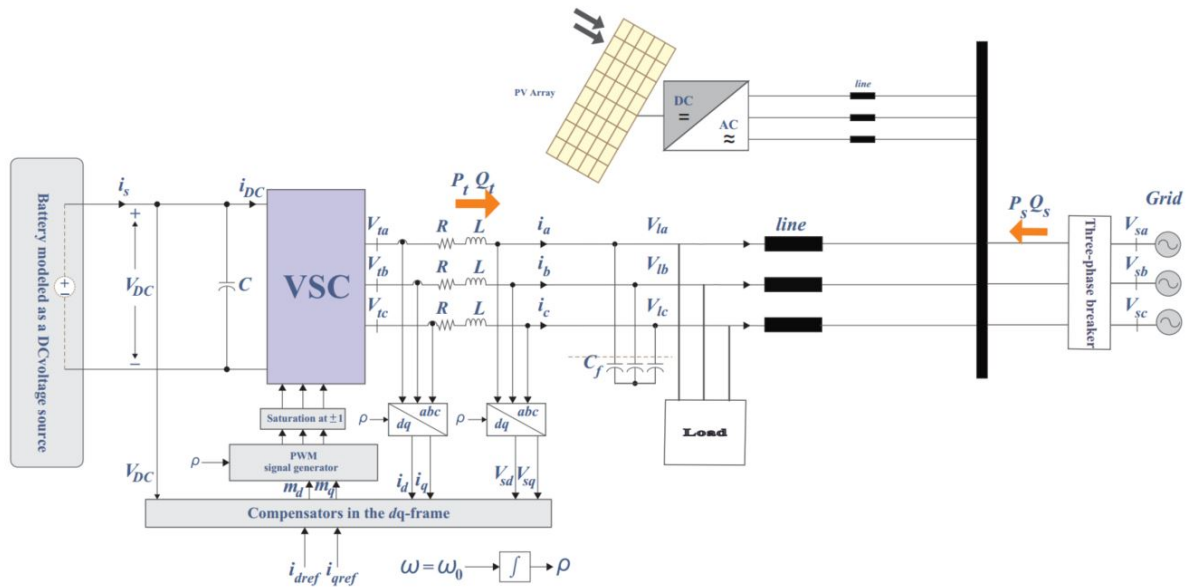


Figure 4.9: The topology of the microgrid with the measurement and control blocks when the three-phase breaker is closed.

In Figure 4.9, the topology of the microgrid is depicted when the three-phase breaker is closed and the microgrid is connected to the main grid. The Figure 4.10 shows the topology of the microgrid after the transition to the stand-alone mode. The voltage and frequency stability of the microgrid depend on the switching mechanism between the two different control strategies corresponding to the two microgrid topologies in Figures 4.9 and 4.10. As was discussed in section 2.6.1, there are mainly three categories of methods which are used for the islanding detection: passive methods, active methods and, ones which require communication. Passive methods rely on monitoring a variable in the system and detect the islanding based on the deviation in the corresponding variable that is going beyond a certain threshold. Although, passive methods are easy to implement; they usually have wide none detected zones (NDZs). Using THD and voltage unbalance method is tricky since selecting the corresponding thresholds is a complicated task due to the system dependency nature of such methods [57]. The active methods inject disturbances into the system and monitor the response of the system to such disturbances to detect the islanding [58]. The NDZ is smaller in active methods; however, they can reduce the power quality of the system. They also require extra implementation of controllers and signal generators which add more complexity to the islanding detection method [59]. Communication-based methods have the smallest NDZ and the highest cost of implementation. The presence of a supervisory system and communication infrastructure to toggle between two control methods is not an option since the minimizing ICT infrastructure is a requirement for this thesis. Based on the literature review in section 2.6.1, local passive islanding methods are the only options that require no means of communication and thus, are appropriate solutions to tackle the problem of switching between two control schemes. The method that is used in this thesis to detect the islanding and switch the control schemes is the combination of OVP/UVP and OFP/UFP methods described in 2.6.1. The OVP/UVP and OFP/UFP methods operate based on voltage and frequency measurements at the point of common coupling. As soon as the measurements exceed the certain thresholds, the islanding detector switches from the current controlled strategy to the frequency controlled strategy.

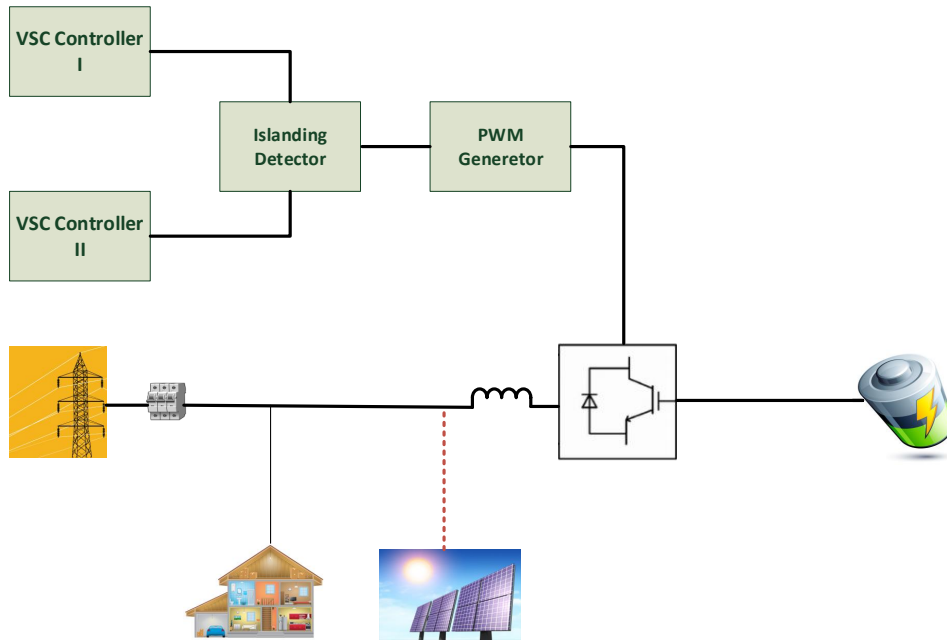


Figure 4.11: The schematic of the microgrid blocks including the islanding detection block.

Equations 4.25 and 4.26 respectively. Inequalities in Equations 4.25 and 4.26 define the NDZ as well, meaning if the microgrid is islanded and the deviation in active power and reactive power is within the following limits, the islanding detector cannot detect the islanding and the control schemes would not be switched.

$$\left(\frac{V}{V_{max}}\right)^2 \leq \frac{\Delta P}{P} \leq \left(\frac{V}{V_{min}}\right)^2 - 1 \quad (4.25)$$

$$Q_f \left[1 - \left(\frac{f}{f_{min}}\right)^2\right] \leq \frac{\Delta Q}{p} \leq Q_f \left[1 - \left(\frac{f}{f_{max}}\right)^2\right] \quad (4.26)$$

The IEEE Std. 1547 defines the acceptable range of output voltage of a distributed generation (DG) unit to be 0.88 pu to 1.1 pu [60]. The range of frequency for a DG unit is defined as 49.2 Hz to 50.3 Hz [61]. If the criteria for islanding detection is defined as being out of this range, any voltage deviation caused by islanding of the microgrid which sits in this range would not be detected as islanding. In other words, the deviations in voltage and frequency are within the NDZ range. The corresponding flowchart to detect islanding by this method could be represented in 4.12.

The effectiveness of this islanding method is investigated of which the results are presented in the next chapter.

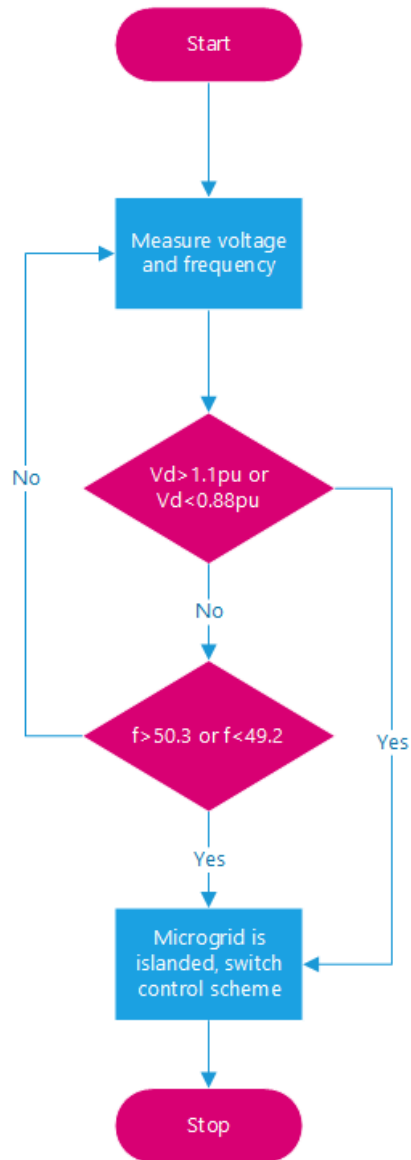


Figure 4.12: The flowchart for the passive islanding detection using OVP/UDP and OFP/UFM methods.

5

Results

5.1. Introduction

In the previous chapter, three main case scenarios were established. For each case scenario, a control scheme was introduced. In this chapter, the simulation results of the implemented control strategies on the developed microgrid model are being investigated in detail. The microgrid should operate stably in both standalone and grid-connected operation of the microgrid. The transition between the two modes should be smooth, meaning the voltage and frequency should be within the predefined limits. The islanding detection decides which mode of the dual controller should be applied to the battery inverter. It is worth mentioning that although a PV array is implemented as a RES in the proposed model of the microgrid in chapter 3; the simulation results in this chapter are found based on no solar irradiation, meaning the only source of energy in the microgrid is the BESS. Omitting all the other resources from the microgrid gives us the opportunity to focus on the behavior of the BESS and the control schemes which are implemented on it.

5.2. Microgrid in Grid Connected Mode of Operation

The controller is designed according to Section 4.2 for the operation in grid-connected mode. A block diagram for the current controller is given in Figure 5.1. The VSC controller in Figure 5.1 consists of a measurement block, a PLL, outer loop active and reactive power controllers together with an inner loop current controller and the PWM generator to control the battery inverter. In this operating condition, the frequency and the voltage at the PCC are imposed by the utility grid. The objective of the controller is to regulate the active and reactive power which are exchanged between the battery inverter and the utility grid at the PCC. The reference active and reactive power is determined by the droop controller and is set to -100 kW and -50 kvar respectively meaning the inverter is supposed to inject power into the grid. P_t and Q_t are the values for active power, and reactive power injected into the PCC from the inverter side, and V_t and f depict the magnitude and the frequency of the voltage at the inverter terminal. V_i and f are dictated by the utility grid. The PLL senses the imposed voltage at the PCC. The PLL locks the quadrature component at zero. Therefore the voltage is just represented by the direct component. Doing so, the I_d and I_q can be decoupled and P_t and Q_t can be controlled by I_d and I_q respectively. Neglecting the start-up transient, the microgrid operates stably in grid connected mode as depicted in Figure 5.2. The simulation is run for 10 s. V_t and f are imposed by the utility grid to have the values of 380 V and 50 Hz respectively. Load disturbances can not alter the the frequency at the PCC as long as the microgrid is connected

to a stiff main grid. Investigating figures 5.3 and 5.3 shows the portion of the active power and reactive power which is injected into the main grid and the loads. The primary controller sets the output power of the battery inverter at 100 kW and 50 kvar respectively. The load consumes 50 kW and 25 kvar, therefore the main grid absorbs 50 kW and 25 kvar as depicted in figures 5.3 and 5.3. The frequency at the inverter terminal and the load terminal is imposed by the grid to be 50 Hz. The voltage at the load terminal is following the voltage at the PCC as expected.

The grid parameters for the simulation of the microgrid in grid-connected operation are defined in Table 5.1. The VSC parameters are defined in Table 5.2 and the variables in the simulation results are defined in Table 5.3.

Table 5.1: The grid parameters for the simulation in grid-connected operation

Parameter	Symbol	Value	Units
Grid Voltage (RMS ph-ph)	V_s	380	V
Grid Frequency	f_s	50	Hz
Grid Inductance	L_s	16.58e-3	H
Grid Resistance	R_s	0.8929	Ω

Table 5.2: The VSC parameters used in the microgrid model

Parameter	Symbol	Value	Units
Snubber resistance	R_{sn}	10^5	Ω
Snubber capacitance	C_{sn}	∞	F

Table 5.3: The microgrid variables

variable	Symbol	Units
Grid active power	P_s	kW
Grid reactive power	Q_s	kvar
VSC active power	P_t	kW
VSC reactive power	Q_t	kvar
VSC terminal voltage	V_t	V
VSC terminal frequency	f_t	Hz
Load active power	P_l	kW
Load reactive power	Q_l	kvar
Load terminal voltage	V_l	V
Load terminal frequency	f_l	Hz

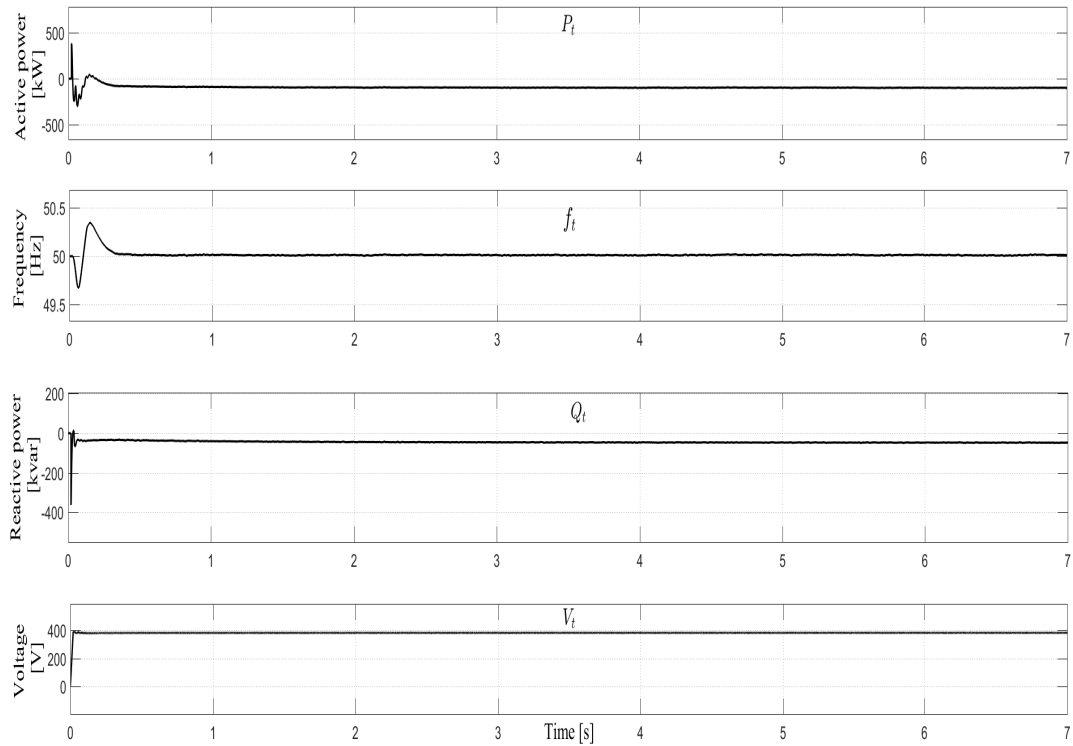


Figure 5.3: Monitoring the voltage, frequency, active and reactive power at the VSC terminal when microgrid is in the grid connected mode of operation and the controller is set to current controlled mode.

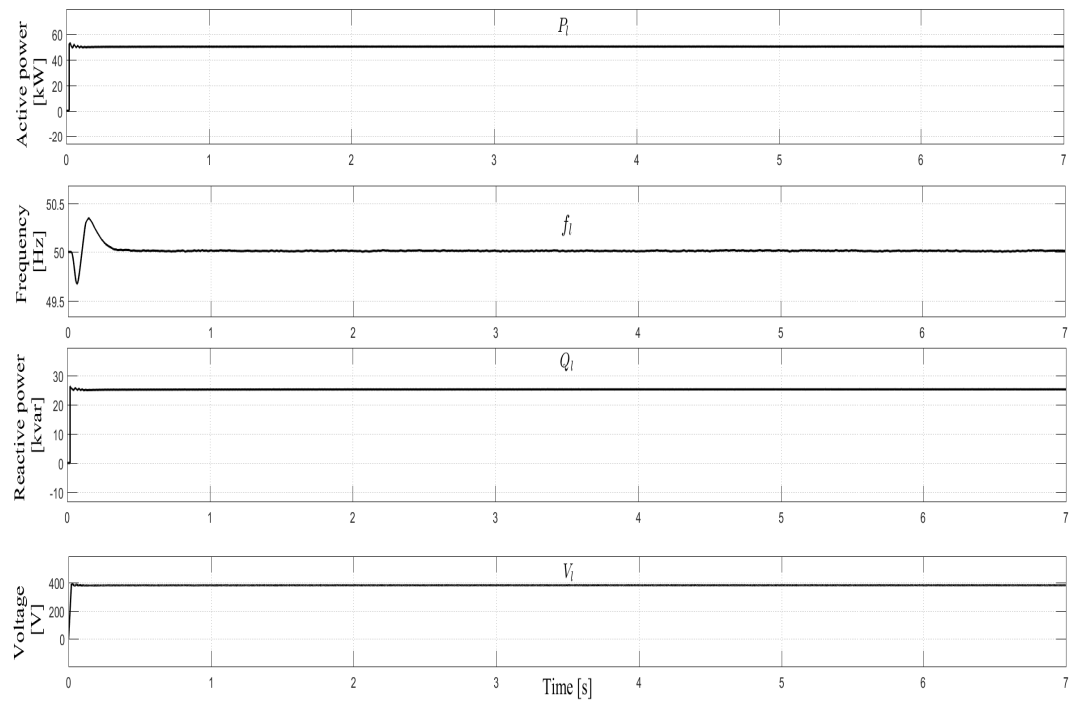


Figure 5.4: Monitoring the voltage, frequency, active and reactive power at the load terminal when microgrid is in the grid connected mode of operation and the controller is set to current controlled mode.

5.3. Microgrid in Stand-alone Mode of Operation

The controller is designed according to the Section 4.3 for the stand-alone operation mode. In this operating mode, the frequency is not imposed at the PCC by the utility grid frequency because it has already been disconnected by a three phase breaker which was implemented in chapter 3. The objective of the voltage/frequency controller is to regulate the voltage and frequency at the PCC, doing so the controller guarantees the loads connected to PCC are provided by a stable voltage and frequency, and the reactive and active power exchange are determined by the loads.

The start-up transient is ignored in this simulation, and therefore the simulation starts at $t = 1$ s. The reference voltage and frequency is set to 380 V and 50 Hz respectively. P_l and Q_l are the values of active power, and reactive power injected into the loads from PCC, and V_l and f_l depict the magnitude and the frequency of the voltage at the PCC which is the same as voltage and frequency at the load terminals. Neglecting the start-up transient, The microgrid operates stably in stand-alone mode as is depicted in Figure 5.5.

The simulation is run for 10 s. However, this time, a 0.2 pu increase in loads is exerted at $t = 3$ s to evaluate the performance of the voltage/frequency controller. As expected the frequency drops after the demand surpasses the power injected into the loads by the battery inverter. The reactive power injected into the loads is also lower than the demand, therefore the V_t and thus V_l drops. The corresponding PI controller which was discussed in Section 4.2.2 senses the error between V_l and V_{lref} and tries to compensate the error. The voltage and frequency overshoot is caused by the proportional and integral gains derived in 4.2.2. In order to have a lower overshoot, one can decrease the proportional gain (K_p) and integral gain (K_i). However, by doing so, the response time of the controller increases. Fine-tuning the PI controller is a trade-off between the response time of the controller and the acceptable overshoot of the V_l . A magnified version of the simulation in Figure 5.6 is given in Figure 5.6 to complement the comprehension of the results. As was mentioned in Chapter 4, the IEEE Std. 1574 defines the acceptable range of output voltage of a distributed generation (DG) unit to be 0.88 pu to 1.1 pu [60] and the range of frequency for a DG unit is defined as 49.2 Hz to 50.3 Hz [61]. The voltage at PCC V_l and frequency at PCC f_l will maintain their nominal values at a fraction of a second (0.1 s) after the disturbance is applied to the loads and the controller restores their values to 380 V and 50 Hz respectively.

Another disturbance is applied at $t = 7$ s at which a 0.2 pu load shedding happens. As expected the frequency increases after the demand is lower than the power injected to the loads by the battery inverter. Due to decreased demand in reactive power, the VSC inverter produces more reactive power than the reactive power which is consumed by the loads. Therefore V_t and thus V_l increase. The corresponding PI controller once again senses the error between V_l and V_{lref} and tries to compensate the error. The voltages show several ripples before it settles because of using the PI compensator. The PI controller can be tuned more tightly to have a faster response in this case however it would affect the voltage overshoot in the previous section in which an increase in load was applied. Just like the first disturbance, V_l and f_l will maintain their nominal values at a fraction of second (0,1 s) after the disturbance is applied to the loads and the controller set their values to 380 V and 50 Hz respectively. The results suggest that the voltage/frequency controller does its job when the microgrid is disconnected from the grid.

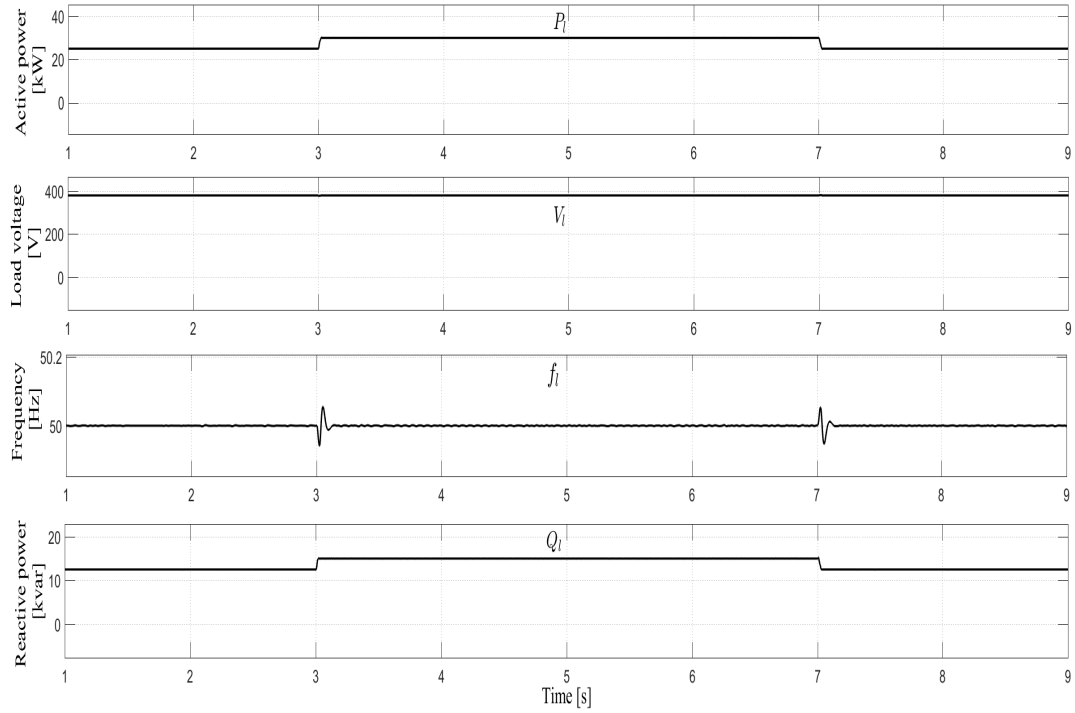


Figure 5.5: Monitoring the voltage, frequency, active and reactive power at load terminals when microgrid is in the stand alone mode of operation and the controller is set to voltage/frequency controlled mode.

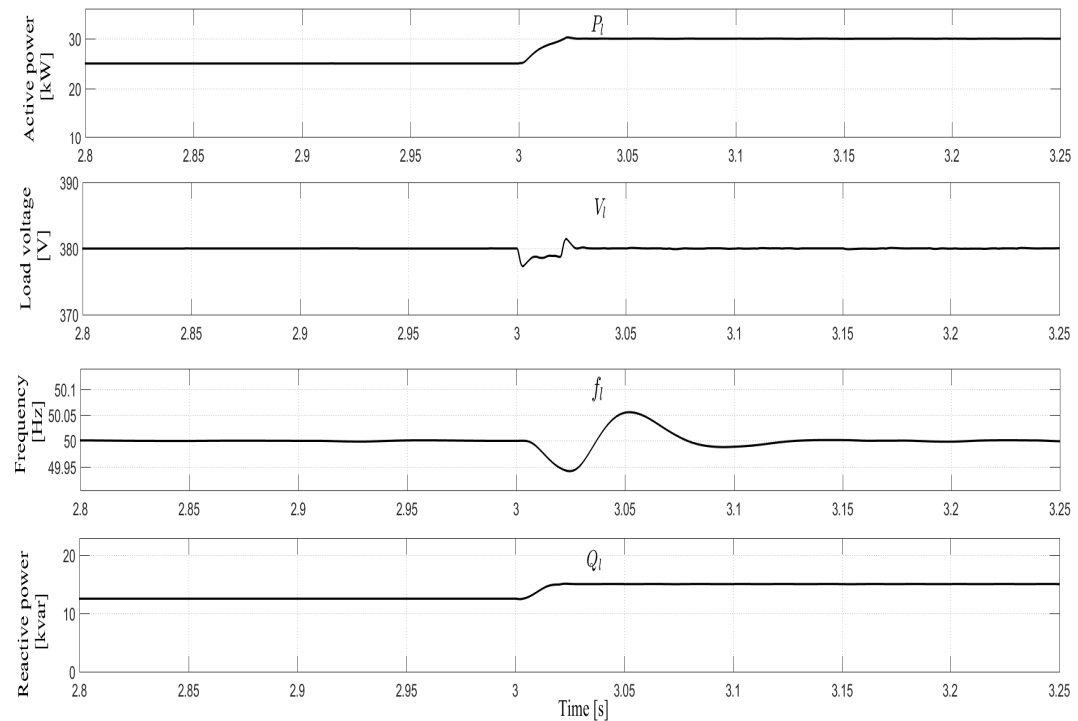


Figure 5.6: Magnified version of Monitoring the voltage, frequency, active and reactive power at load terminals when microgrid is in the stand alone mode of operation and the controller is set to voltage/frequency controlled mode while a disturbance in the load is applied.

5.4. Microgrid in Transition Between Operations without the Implementation of Dual-controller

This section justifies the necessity for a dual-controller since the current controller can not stabilize the microgrid when it is disconnected from the main grid and the voltage/frequency controller is not able to control the active power, and reactive power exchanged between the battery inverter and the PCC when the microgrid is connected to the grid.

For the first 3 seconds of the simulation, the microgrid operates in grid connected mode, and the VSC controller operates just like the Section 5.1. The three phase breaker disconnects the microgrid from the utility grid at $t = 3$ s. The microgrid operates in islanding mode without the presence of the islanding detection. Figure 5.7 shows the voltage and frequency dynamics at the grid side. The reference values for the active and reactive power of the battery VSC are set at -100 kW and -50 kvar respectively. The load consumes 50 kW and 25 kvar so 50 kW and 25 kvar should be absorbed by the utility grid when the microgrid is connected to the grid. When the grid is disconnected, the excess power generated by the battery inverter cannot be injected into the grid anymore. The voltage and frequency dynamics at the battery inverter are depicted in Figure 5.8 and the voltage and frequency dynamics at the load terminal are depicted in Figure 5.9. The load is modeled as a constant-impedance to monitor the dynamics at the load terminals easier. Both P_t and Q_t are decreased by the primary control; however, P_t and Q_t are still higher than their nominal values due to the absence of the grid connection. The excess active and reactive power injected into the PCC from the BESS side cause the voltage and frequency at the PCC to increase. The PI controllers which are implemented in outer active and the reactive power controller in 5.1 try to damp the error between the reference values and their measured values. Therefore both active and reactive power which are injected into the PCC from the BESS decrease. The current regulator block fails to stabilize the voltage and frequency because according to the Equation 4.6, i_{dref} and i_{qref} are dependant on both the reference active power and reactive power and also the direct component of the voltage at the PCC. When the microgrid is disconnected, V_{sd} and therefore V_{ld} , can not be considered as constant values anymore, so the decoupled control scheme which was the basic assumption in the current controlled mode is not valid. P_t and Q_t will pass their reference values due to the fact that the decoupled control scheme considers the V_{ld} to be fixed at nominal voltage and V_{lq} at zero which is not applicable anymore. The active and reactive power will damp to zero, and the voltage and frequency at the PCC will be zero based on the active and reactive power which cause the magnitude and frequency of the VSC terminal voltage to go out of the allowed margins. After few seconds, V_t is forced to zero as a result of no active and reactive power injection from the inverter side. The simulation results in Figure 5.8 suggests that a different control scheme should be implemented to stabilize the microgrid when the microgrid is disconnected from the utility grid. The required control scheme when the microgrid is disconnected from the utility grid is the voltage/frequency controlled scheme which was designed in Section 4.2.2 and implemented in Section 5.3. Switching to the aforementioned control technique requires a mechanism to toggle from one control scheme to the other. The issue of toggling between two control schemes was addressed in Section 4.2.3.

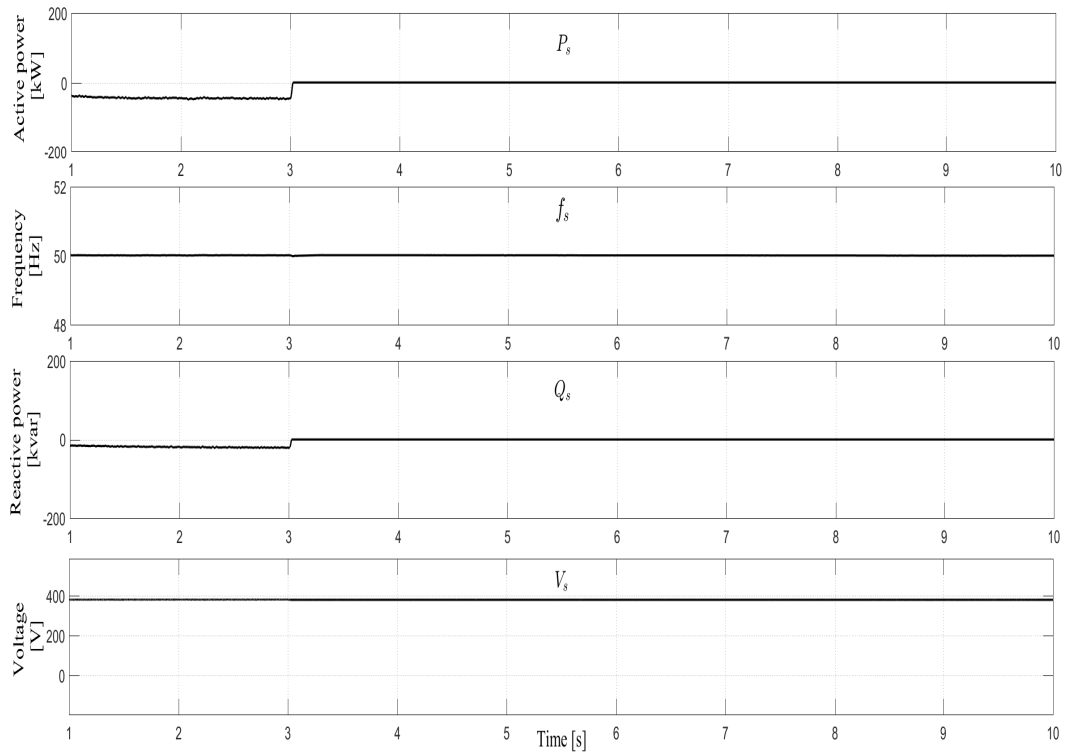


Figure 5.7: Monitoring the voltage, frequency, active and reactive power at utility grid side when the microgrid is in transition between grid connected and stand-alone modes of operation without switching between the controllers.

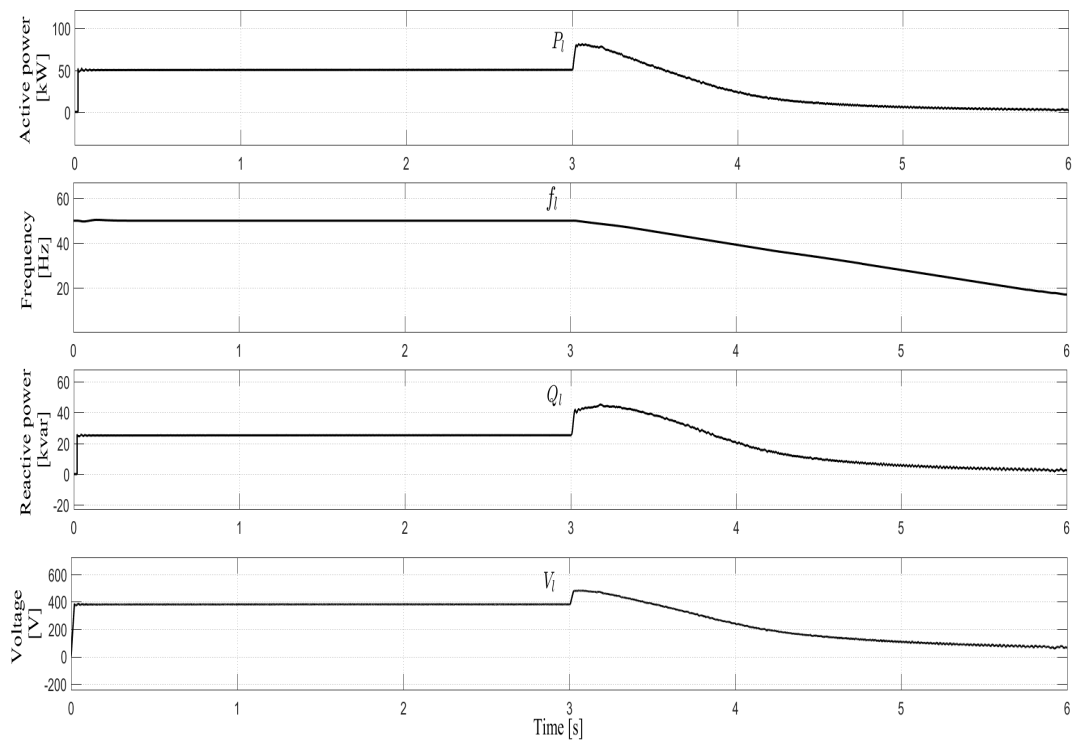


Figure 5.8: Monitoring the voltage, frequency, active and reactive power at the VSC terminal when the microgrid is in transition between grid connected and stand-alone modes of operation without switching between the controllers.

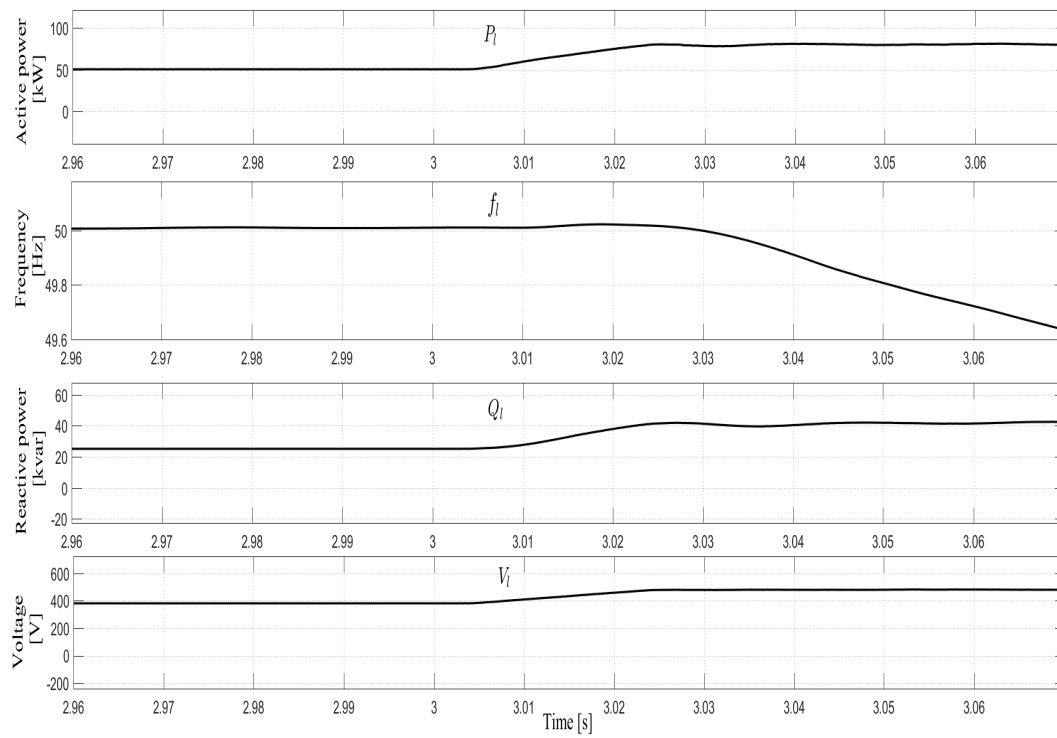


Figure 5.9: Monitoring the voltage, frequency, active and reactive power at load terminal when the microgrid is in transition between grid connected and stand-alone modes of operation without switching between the controllers.

5.5. Microgrid in Transition Mode Between Operations Modes with Dual-controller Implemented

The controller is designed as a combination of the two controllers in previous sections together with an islanding detection block represented in Section 4.2.3. As long as the islanding detection detects no means of disturbance in voltage and frequency at the PCC based on the islanding criteria implemented in the corresponding block defined in 4.2.3, the dual controller operates as a frequency imposed controller taking control of the active and reactive power exchange with the utility grid. As soon as the islanding detection diagnoses a huge disturbance defined by the islanding criteria in either voltage magnitude or frequency, the control scheme is switched to voltage/frequency controlled mode. In such a condition, the objective of the controller is suddenly changed from controlling the active and reactive power to controlling the frequency and magnitude of the voltage at the PCC. To simulate this operating condition, the same three phase breaker proposed in Chapter 3 is used to model the islanding. The microgrid starts to operate in the grid-connected mode, and the islanding detection chooses the frequency imposed strategy to be implemented on the battery bank inverter to control the active and reactive power at PCC. At $t = 4$ s the three phase breaker disconnects the utility grid, the same breaker will connect the microgrid to the utility grid at $t = 7$ s. Subsequent to the islanding of the microgrid, the islanding detection diagnoses an off limit disturbance in the frequency at the PCC; therefore the detection block changes the control scheme to voltage/frequency controlled mode, and the battery inverter controls the voltage and frequency at PCC which was imposed by the utility grid before the islanding. The primary control sets the reference of the battery inverter at -100 kW and -12.5 kvar. The load is modeled as a constant impedance load with rated at 25 kW and 12.5 kvar. Based on the loads and reference values for active and reactive power of the inverter, there should be no reactive power exchange with the utility grid when the microgrid is connected to the grid. The results in figure 5.10 shows no reactive power exchange as expected. The frequency and the voltage at the grid side are not affected by the islanding of the microgrid. When the microgrid is disconnected from the main grid, there is 75 kW additional power which produced by the battery inverter but can not be absorbed by the utility grid. The excess active power generation increases the frequency at the PCC, and the islanding detection senses the frequency jump. The control scheme is switched to voltage/frequency control mode. The voltage at the PCC drops subsequent to the islanding. The voltage/frequency controller restores the voltage to its nominal value by increasing the I_d . The frequency shows a well-damped response caused by the implemented PI controller. The response of the controller to the islanding event can be seen at the PCC in Figure 5.11. Prior to $t = 7$ s, the microgrid is in steady state. The voltage/frequency control scheme has locked the quadrature component of V_{tq} at zero. After the connection to grid, the control scheme is switched to frequency imposed mode allowing the grid to dictate the voltage and frequency at the PCC. The reference active and reactive power should be injected into the PCC by the battery inverter. The outer power loop senses the difference between the reference active power and its measured value. The error between the two values is damped by the PI controller in the corresponding block. As the active power generation restores its reference value, the frequency settles at 50 Hz. The reactive power control loop damps the reactive power because there should be no reactive power exchanged with the grid based on the primary control. The momentary voltage drop which was caused by switching between two control schemes is restored by the grid, and the microgrid goes to the steady state.

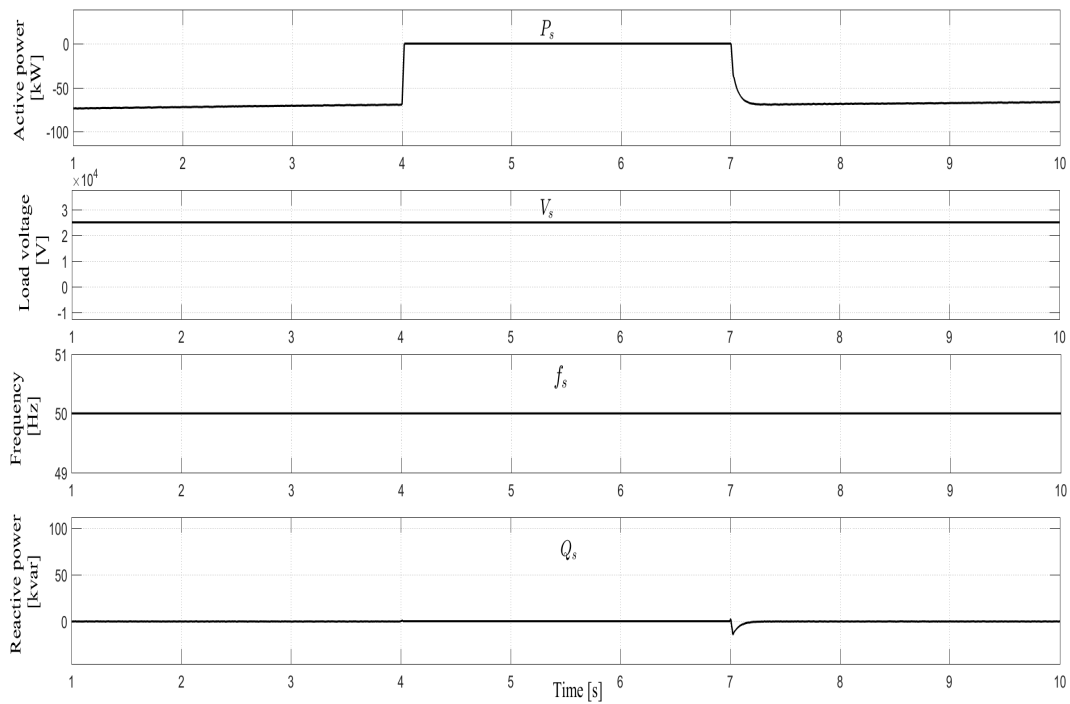


Figure 5.10: Monitoring the voltage, frequency, active and reactive power at utility grid side when microgrid is in transition between grid connected and stand alone mode of operation, and the controller is set to dual control mode with islanding detection.

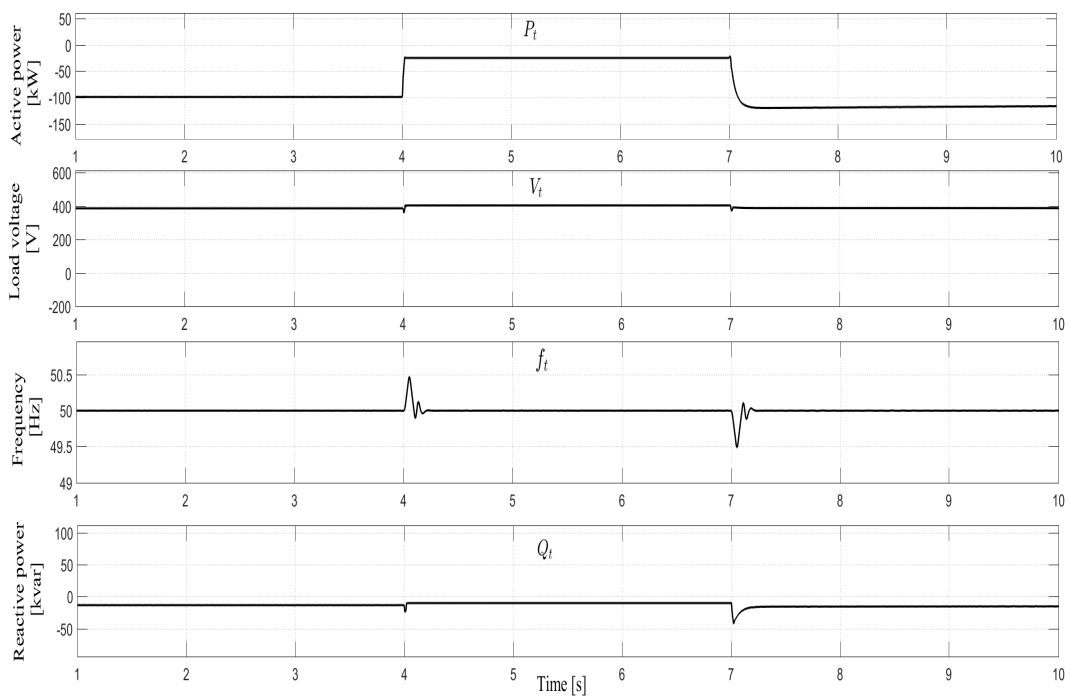


Figure 5.11: Monitoring the voltage, frequency, active and reactive power at load terminals when microgrid is in transition between grid connected and stand alone mode of operation and the controller is set to dual control mode with islanding detection.

5.6. Evaluation of the Control Scheme

The main objective of this thesis was to design a battery controller which can run the microgrid model in both islanded and grid-connected mode, but more importantly to guarantee a smooth transition between two operation modes with the minimum presence of ICT infrastructure. In Chapter 4, a decentralized control strategy was proposed to control the battery banks in the microgrid model based on the readily available parameters (voltage and frequency). The objective of the control strategy was to maintain the active and reactive power injected from the battery inverter side into the PCC when the microgrid is connected to the utility grid and to support the frequency and voltage at the PCC when the microgrid operates in stand-alone mode. Based on the simulations, the designed controller fulfills all the listed objectives in the project description. In a nutshell, the control scheme senses the behavior of the grid at the PCC and adapts the control methods applied on the VSC of the BESS accordingly without receiving any upstream signal from the grid side. The effectiveness of this method can only be judged by comparing the dual-control strategy to the communication-based control strategies (centralized control) which are recommended in the literature. The advantages of using a decentralized control without the supervisory control can be summarized as follows:

- Lower costs: The control system would be much cheaper without using complicated components to monitor and measure the microgrid variables and to send them to the central controller. There is no need to construct communication lines and cables which reduces the implementation cost of the controller dramatically.
- Less complex architecture: The absence of communication-based components makes the control system less complicated and easier to understand.
- Higher reliability: In a centralized scheme, the whole system can fail due to either the failure of the electrical network or the failure of the communication network whereas, by using a decentralized control scheme, the availability of the electricity is only dependant on the reliability of the electrical grid. It is worth mentioning that the reliability of an electrical grid is much higher than any given communication grid.
- Higher scalability: By applying local controllers, expanding the microgrid would be much simpler because there is no need to construct extra communication lines and components when a new actor has entered the microgrid. In fact, using a decentralized control facilitates the implementation of the plug and play actors in the microgrid.
- Less delay: Although using the islanding detection block adds a delay to the response of the controller, the delay is significantly smaller than the delay of the communication systems.
- Less vulnerability to noise: Communication lines are subject to external noise whereas a local controller is much more immune to external noise.

In order to compare the level of complexity of using a central controller to the proposed local controller, the hardware structure of a BESS using a central controller is given in Figure 5.12, and the hardware structure of a BESS using a decentralized controller is depicted in Figure 5.13.

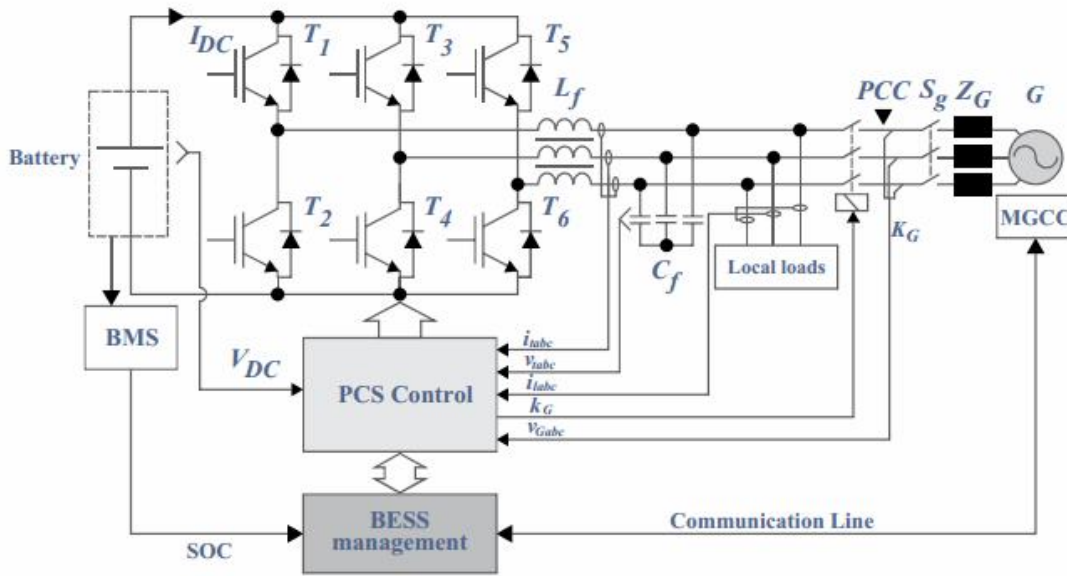


Figure 5.12: The topology of the battery controller with the presence of microgrid central controller and communication infrastructure.

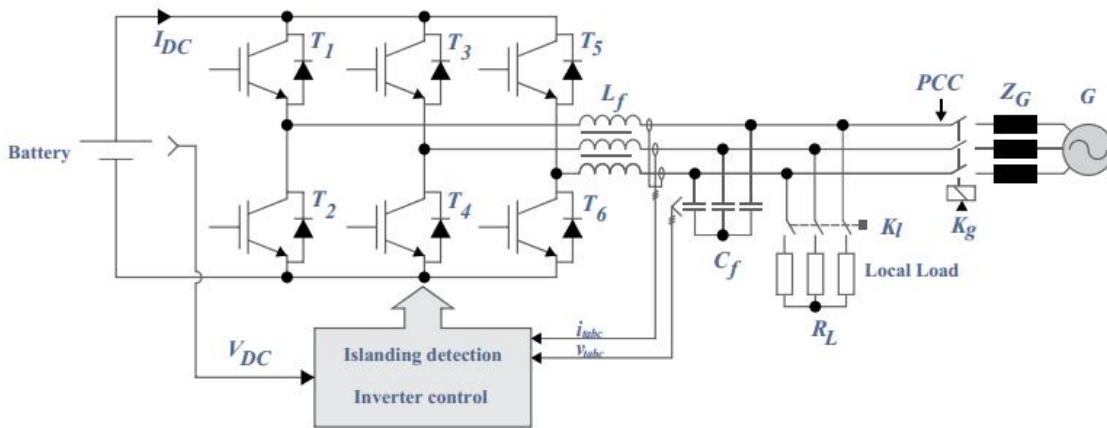


Figure 5.13: The topology of the battery controller with no means of communication infrastructure.

The presence of the battery management system (BMS) to provide the set-points based on the SOC of the batteries to the BESS management and communication lines between the MGCC and the BESS management adds another level of complexity to the control structure. Utilizing the communication lines eliminates the need for a local islanding detection technique. However, an upstream signal is required from the utility grid to switch the control strategy when the microgrid is disconnected from the main grid. The obvious advantage of using such a structure is to eliminate the chance of not detecting the islanding because of the NDZs in the passive islanding method used to switch between control strategies. The power conversion system (PCS) is responsible for controlling the batteries VSC like the inverter control block

in Figure 5.13 with the exception of getting additional measured signals compared to the decentralized controller. Aside from the extra hardware complexity in the implementation of centralized control schemes, the control complexity is also increased by utilizing additional input signals.

The advantages of using a centralized approach can be considered as the disadvantages of using the proposed dual-control scheme which are listed as follows:

- NDZ: None detected zones (NDZs) are the main Achilles heels of using the dual-control strategy. Although based on the simulation results, there was no disturbance in the microgrid during the grid-connected operation that was misinterpreted as the islanding criteria; there could be a condition in which the islanding is fell under the NDZ when a passive islanding detection method is utilized. The combination of OVP/UVP and OFP/UFP methods which are implemented in this thesis narrows down the NDZ but does not eliminate the chance of having one.
- Non adaptive control: The controller does not change the reference set points based on the SOC of the battery.
- Over-simplification: The impedance of the cables which connect the loads to the AC side of the microgrid is neglected because no signals should be sent from the load side to battery controller. Therefore the voltage at the load terminal is considered to be the same as the voltage at capacitive filters.
- Connection to other microgrid cells: In the conducted research, the connection of the microgrid to the other microgrid cells was not considered. In fact, to connect the microgrid to other microgrid cells a DC or an AC backbone is needed. This backbone can be connected to the grid as well. Therefore the variations in voltage and frequency can also be caused by the dynamics of the voltage and frequency in other microgrid cells when they are connected through a backbone. The consideration of such a backbone is out of the scope of this thesis.

6

Conclusions and Future Work

In the previous chapters, I justified a need for a dual-control method scheme to be applied to microgrids with BESS to ensure a secure operation in the grid-connected mode as well as the stand-alone mode. I also showed that such control scheme enables a smooth transition between the two operating modes. Subsequently, I presented simulation results to demonstrate the effectiveness of the proposed control strategies in microgrids.

This chapter summarizes the answers to the research questions and revisits the main contributions of this thesis. It also presents a list of relevant conclusions arising from the research that was performed in each Chapter. Finally, some proposals for future research are made.

6.1. Contributions

As the primary application of the SOPRA cells was to provide electricity to rural consumers, the connection to the main grid was not investigated nor provisioned. Thus, the SOPRA cells were considered as stand-alone systems. CSGriP aims to extend the application of SOPRA cells to enable grid-connected mode as well as cell to cell connected mode. An adequate control strategy is needed to support the voltage and frequency at the point of common coupling (PCC) in both the grid-connected and the stand-alone modes to allow a stable active and reactive power sharing. In addition, the transition between the two modes of operation is of great importance to ensure voltage and frequency stability, regardless of operating mode understudy.

The CSGriP is considered as the expansion of the SOPRA project to introduce a modular microgrid concept with the option to connect to the main grid.

In summary, my contributions in this thesis are as follows:

6.1.1. Microgrid Modeling

The control scheme methodology is tested on a microgrid that consists of a PV array, BESS, different types of loads, and the required transformer, cables and filters.

The microgrid is assumed to connect to the main grid via a three-phase breaker. The breakers are considered open during islanding mode.

The parameters of the generic battery model were modified to represent the Li-Ion batteries. The control schemes were implemented in the controller of the voltage source converter (VSC) converter which is the interface between the DC link connecting the battery system to the AC grid. Note that; the project description dictates using minimum ICT infrastructure. Therefore, any control scheme that relies on communication lines cannot be considered as an option.

6.1.2. Control Schemes

Two control schemes were developed in this thesis. In addition, a hybrid islanding detection block is used to combine the two control schemes to tackle the stability issue of the microgrid during the transition between two operation modes.

The controller of VSC of the BESS in the grid-connected operation model, is based on the decoupling of current components of the inverters (I_d and I_q). This is done by setting the quadrature component of the voltage at PCC to zero using a PLL.

Projecting the voltage at the PCC on the direct axis of dq transformation provides the opportunity to control the output active power and reactive power of the VSC using I_d and I_q , respectively. When the microgrid is in islanded operation mode, V_l is not dictated by the grid anymore. Under such condition, similar idea as the one used to control the battery inverter during grid-operation regarding the PLL should be considered to keep the quadrature component of the voltage (V_{lq}) at zero. This holds true, even when the V_l is not imposed by the stiff grid. The dynamic of V_{ld} and V_{lq} are coupled. This issue is solved using feed-forward signals by decoupling the direct and quadrature components of the voltage. Therefore, the voltage control at PCC is achieved by controlling the I_{dref} and I_{qref} . Lastly, an islanding detection block is considered to ensure a smooth transition between the two control schemes.

6.1.3. Control Scheme Verification

The simulation results in Chapter 5, demonstrate that the proposed control scheme responds analogously in both operation modes. The PCC voltage is shown to track the reference value in less than 10 ms. This represents a well-damped response. Finally, the simulations also show that V_{lq} remains unchanged subsequent to a change in V_{ld} . This observation proves the efficiency of the proposed dynamic decoupling method.

For the stand-alone operation mode, I investigated the response of the system to a sudden change in the load. I observe that the voltage at PCC tracks the reference in under 10 ms, when there is either a jump in the load or a load shedding.

The islanding detection is the block that links the switches between the two control strategies. When the microgrid is disconnected from the utility grid, the islanding detection is proved to be able to recognize the transition state. The range of variation in voltage and frequency are within limits ensuring a smooth transition between two operation modes.

The simulation results verify the application of the designed controller in both the grid-connected, and the islanded operation modes. The transition between the two operation modes is smooth in terms of voltage and frequency.

As was discussed in Chapter 5, the controller has lower implementation cost, less complicated architecture, and higher reliability and scalability compared to control methods that use communication and coordinated structures. Any control system relying on communication is prone to having more delay and noise interferences compared to a control scheme that is solely based on locally available signals, such as the one proposed in this work.

Forming the model based on actual branch parameters for AC and DC power flows allows for accounting for voltage drop over cables connecting the loads to the AC side. This enables a more accurate modeling of microgrid control.

The islanding detection block is observed to have a non-discovery zone (NDZ). This characteristic is considered as the main disadvantage of the proposed control scheme. The control scheme is less adaptive compared to coordinated control strategies and does not include the state of the PV inverter and the temperature effect in the battery banks.

One key issue is the connection between microgrid cells in the scope of CSGriP project. This topic falls out of the scope of this thesis. This issue has been studied in parallel to this work.

Last but not least, the proposed micro grid model has limitations which have to be considered. For example, approximating the stiff utility grid with a three phase voltage source fails to capture several characteristics of the grid that are important in reality such as the existence of high rotational inertia. Moreover, as the energy meters in the microgrid cannot send their parameters by a communication line to the inverter control, the impedance of the cable which connects the loads to the PCC is neglected.

6.2. Future Work

In the future, the proposed control scheme could be further developed in the direction to focus on improving the weak points of the dual-controller, as are discussed in Chapter 6.1.3.

Another extension could be to work on the NDZ issue. This problem can be addressed by adding another layer of passive islanding detection block. Note that this issue can be solved completely only by implementing a communication-based method. Therefore another area for future research could be to compare the performance of the proposed methodology, with a communication-based model.

One possible solution to tackle the problem of “over-simplification of reading the microgrid parameters” is to add a certain level of low-bandwidth communication (LBC) link to the microgrid model. Even then, there would be no upstream signal from the main grid to the BESS. Therefore, the islanding detection technique uses proposed in this thesis, remains responsible for adapting the control modes of the battery inverter regardless of whether the microgrid being connected to the stiff grid or not. For this case, a more BESS model is required. One suggestion for BESS is as presented in Figure 6.1.

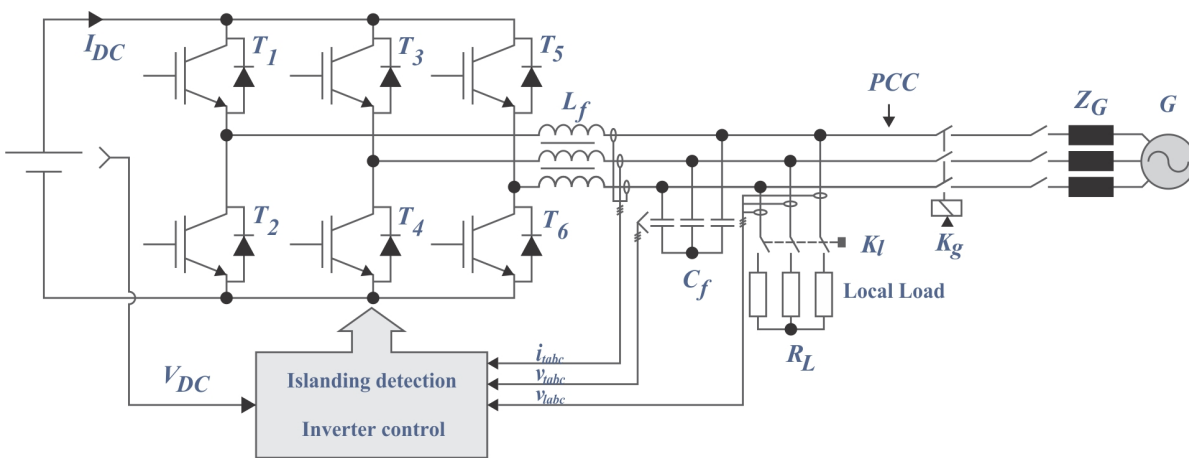


Figure 6.1: The modified topology of the battery controller with the implementation of low-bandwidth communication to measure the load terminal voltage

One can see an extra LBC connection that transmits the measured voltage at the load terminals to the VSC controller. Adding the new LBC connection is expected to improve the performance of the control module. This is because of the additional information regarding the voltage drops over cables connecting the loads that are transmitted to the PCC. It is of interest to investigate the effectiveness of the proposed BESS model.

6.3. Concurrent Works

Several other research topics have been defined within the scope of CSGriP project as follows:

1. Optimal sizing of a CSGriP cell by solving an optimization problem in the GAMS software.
2. Demand side management using CSGriP frequency.
3. Virtual inertia implementation in a CSGriP cell.
4. Investigating the connection of several CSGriP cells to each other.

The methodology developed and the simulations implemented in each project can be merged with the BESS control strategy that is developed in this thesis. This would lay down the foundations of a comprehensive study that investigates the challenges and solutions towards realizing a cellular microgrid.

Bibliography

- [1] Q. C. Zhong and G. C. Konstantopoulos, *Nonlinear current-limiting control for grid-tied inverters*, in [2016 American Control Conference \(ACC\)](#) (2016) pp. 7472–7477.
- [2] I. Serban and C. Marinescu, *An enhanced three-phase battery energy storage system for frequency control in microgrids*, in [Optimization of Electrical and Electronic Equipment \(OPTIM\), 2012 13th International Conference on](#) (2012) pp. 912–918.
- [3] A. Bidram, A. Davoudi, F. L. Lewis, and J. M. Guerrero, *Distributed cooperative secondary control of microgrids using feedback linearization*, *IEEE Transactions on Power Systems* **28**, 3462 (2013).
- [4] P. O. Kriett and M. Salani, *Optimal control of a residential microgrid*, *Energy* **42**, 321 (2012).
- [5] E. Planas, J. Andreu, J. I. Gárate, I. M. de Alegría, and E. Ibarra, *Ac and dc technology in microgrids: A review*, *Renewable and Sustainable Energy Reviews* **43**, 726 (2015).
- [6] C. Colson, M. Nehrir, and R. Gunderson, *Distributed multi-agent microgrids: a decentralized approach to resilient power system self-healing*, in *Resilient Control Systems (ISRCS), 2011 4th International Symposium on* (IEEE, 2011) pp. 83–88.
- [7] S. Rivera, A. M. Farid, and K. Youcef-Toumi, *A multi-agent system transient stability platform for resilient self-healing operation of multiple microgrids*, in *Innovative Smart Grid Technologies Conference (ISGT), 2014 IEEE PES* (IEEE, 2014) pp. 1–5.
- [8] I. A. Hiskens and E. M. Fleming, *Control of inverter-connected sources in autonomous microgrids*, in [2008 American Control Conference](#) (2008) pp. 586–590.
- [9] J. Sridhar, *Frequency-based energy management using smart meters for sopra*, .
- [10] T. Vral, *Frequency-based microgrid control*, .
- [11] W. Y. Teoh and C. W. Tan, *An overview of islanding detection methods in photovoltaic systems*, *World Academy of Science, Engineering and Technology* **58**, 674 (2011).
- [12] T. L. Vandoorn, B. Meersman, J. D. De Kooning, and L. Vandeveldel, *Transition from islanded to grid-connected mode of microgrids with voltage-based droop control*, *IEEE transactions on power systems* **28**, 2545 (2013).
- [13] W. R. Issa, M. A. Abusara, and S. M. Sharkh, *Control of transient power during unintentional islanding of microgrids*, [IEEE Transactions on Power Electronics](#) **30**, 4573 (2015).
- [14] F. Katiraei and M. R. Iravani, *Power management strategies for a microgrid with multiple distributed generation units*, [IEEE Transactions on Power Systems](#) **21**, 1821 (2006).
- [15] F. Katiraei and M. R. Iravani, *Power management strategies for a microgrid with multiple distributed generation units*, [IEEE Transactions on Power Systems](#) **21**, 1821 (2006).

- [16] A. Mehrizi-Sani and R. Iravani, *Potential-function based control of a microgrid in islanded and grid-connected modes*, *IEEE Transactions on Power Systems* **25**, 1883 (2010).
- [17] J. A. P. Lopes, C. L. Moreira, and A. G. Madureira, *Defining control strategies for microgrids islanded operation*, *IEEE Transactions on Power Systems* **21**, 916 (2006).
- [18] S. Baudoin, I. Vechiu, and H. Camblong, *A review of voltage and frequency control strategies for islanded microgrid*, in *System Theory, Control and Computing (ICSTCC), 2012 16th International Conference on* (2012) pp. 1–5.
- [19] M. Ilic and S. Liu, *Hierarchical power systems control: its value in a changing industry* (Springer Science & Business Media, 2012).
- [20] F. Gao and M. R. Iravani, *A control strategy for a distributed generation unit in grid-connected and autonomous modes of operation*, *IEEE Transactions on Power Delivery* **23**, 850 (2008).
- [21] I. Serban and C. Marinescu, *A look at the role and main topologies of battery energy storage systems for integration in autonomous microgrids*, in *Optimization of Electrical and Electronic Equipment (OPTIM), 2010 12th International Conference on* (2010) pp. 1186–1191.
- [22] M. C. Chandorkar, D. M. Divan, and R. Adapa, *Control of parallel connected inverters in standalone ac supply systems*, *IEEE Transactions on Industry Applications* **29**, 136 (1993).
- [23] A. Chaouachi, R. M. Kamel, and K. Nagasaka, *Microgrid efficiency enhancement based on neuro-fuzzy mppt control for photovoltaic generator*, in *Photovoltaic Specialists Conference (PVSC), 2010 35th IEEE* (2010) pp. 002889–002894.
- [24] A. Keyhani and M. Marwali, *Smart power grids 2011* (Springer, 2012).
- [25] M. H. Ashourian, A. A. M. Zin, A. S. Mokhtar, S. J. Mirazimi, and Z. Muda, *Controlling and modeling power-electronic interface ders in islanding mode operation micro grid*, in *Industrial Electronics and Applications (ISIEA), 2011 IEEE Symposium on* (2011) pp. 161–166.
- [26] M. Mahmoud, S. A. Hussain, and M. Abido, *Modeling and control of microgrid: An overview*, *Journal of the Franklin Institute* **351**, 2822 (2014).
- [27] M. R. Miveh, M. F. Rahmat, A. A. Ghadimi, and M. W. Mustafa, *Power quality improvement in autonomous microgrids using multi-functional voltage source inverters: A comprehensive review*, *Journal of Power Electronics* **15**, 1054 (2015).
- [28] J. M. Guerrero, M. Chandorkar, T. L. Lee, and P. C. Loh, *Advanced control architectures for intelligent microgrids x2014;part i: Decentralized and hierarchical control*, *IEEE Transactions on Industrial Electronics* **60**, 1254 (2013).
- [29] A. Bidram and A. Davoudi, *Hierarchical structure of microgrids control system*, *IEEE Transactions on Smart Grid* **3**, 1963 (2012).
- [30] I. Serban and C. Marinescu, *Control strategy of three-phase battery energy storage systems for frequency support in microgrids and with uninterrupted supply of local loads*, *IEEE Transactions on Power Electronics* **29**, 5010 (2014).

- [31] I. Serban and C. Marinescu, *An enhanced three-phase battery energy storage system for frequency control in microgrids*, in *Optimization of Electrical and Electronic Equipment (OPTIM), 2012 13th International Conference on* (2012) pp. 912–918.
- [32] X. Tan, Q. Li, and H. Wang, *Advances and trends of energy storage technology in microgrid*, *International Journal of Electrical Power & Energy Systems* **44**, 179 (2013).
- [33] B. Roberts, *Capturing grid power*, *IEEE Power and Energy Magazine* **7**, 32 (2009).
- [34] N. Garimella and N.-K. C. Nair, *Assessment of battery energy storage systems for small-scale renewable energy integration*, in *TENCON 2009-2009 IEEE Region 10 Conference* (IEEE, 2009) pp. 1–6.
- [35] B. Yang, Y. Makarov, J. Desteese, V. Viswanathan, P. Nyeng, B. McManus, and J. Pease, *On the use of energy storage technologies for regulation services in electric power systems with significant penetration of wind energy*, in *2008 5th International Conference on the European Electricity Market* (IEEE, 2008) pp. 1–6.
- [36] W. Li and G. Joos, *Performance comparison of aggregated and distributed energy storage systems in a wind farm for wind power fluctuation suppression*, in *Power Engineering Society General Meeting, 2007. IEEE* (2007) pp. 1–6.
- [37] K. S. Kook, K. J. McKenzie, Y. Liu, and S. Atcitty, *A study on applications of energy storage for the wind power operation in power systems*, in *2006 IEEE Power Engineering Society General Meeting* (2006) pp. 5 pp.–.
- [38] J. Liu and N. Henze, *Reliability consideration of low-power grid-tied inverter for photovoltaic application*, in *24th European Photovoltaic Solar Energy Conference, Hamburg, Germany, September* (Citeseer, 2009) pp. 21–25.
- [39] V. Salas, M. Alonso-Abella, E. Olias, F. Chenlo, and A. Barrado, *Dc current injection into the network from pv inverters of < 5kw for low-voltage small grid-connected pv systems*, *Solar energy materials and solar cells* **91**, 801 (2007).
- [40] N. Hatziairgiyriou, H. Asano, R. Iravani, and C. Marnay, *Microgrids*, *IEEE power and energy magazine* **5**, 78 (2007).
- [41] A. Engler, C. Hardt, P. Strauss, and M. Vandenberg, *Parallel operation of generators for standalone single phase hybrid systems—first implementation of a new technology*, in *17th European PV Conference* (2001).
- [42] A. Khamis, H. Shareef, E. Bizkevelci, and T. Khatib, *A review of islanding detection techniques for renewable distributed generation systems*, *Renewable and sustainable energy reviews* **28**, 483 (2013).
- [43] A. Timbus, A. Oudalov, and C. N. M. Ho, *Islanding detection in smart grids*, in *2010 IEEE Energy Conversion Congress and Exposition* (2010) pp. 3631–3637.
- [44] A. Llaría, O. Curea, J. Jiménez, and H. Camblong, *Survey on microgrids: unplanned islanding and related inverter control techniques*, *Renewable energy* **36**, 2052 (2011).
- [45] V. Menon and M. H. Nehrir, *A hybrid islanding detection technique using voltage unbalance and frequency set point*, *IEEE Transactions on Power Systems* **22**, 442 (2007).

- [46] C. Li, C. Cao, Y. Cao, Y. Kuang, L. Zeng, and B. Fang, *A review of islanding detection methods for microgrid*, *Renewable and Sustainable Energy Reviews* **35**, 211 (2014).
- [47] O. Tremblay and L.-A. Dessaint, *Experimental validation of a battery dynamic model for ev applications*, *World Electric Vehicle Journal* **3**, 1 (2009).
- [48] C. Zhu, X. Li, L. Song, and L. Xiang, *Development of a theoretically based thermal model for lithium ion battery pack*, *Journal of Power Sources* **223**, 155 (2013).
- [49] L. Xu, *Modeling, analysis and control of voltage-source converter in microgrids and hvdc*, (2013).
- [50] K.-H. Kim, N.-J. Park, and D.-S. Hyun, *Advanced synchronous reference frame controller for three-phase ups powering unbalanced and nonlinear loads*, in *2005 IEEE 36th Power Electronics Specialists Conference (IEEE, 2005)* pp. 1699–1704.
- [51] K. Areerak, S. Bozhko, G. Asher, and D. Thomas, *Dq-transformation approach for modelling and stability analysis of ac-dc power system with controlled pwm rectifier and constant power loads*, in *Power electronics and motion control conference, 2008. EPE-PEMC 2008. 13th (IEEE, 2008)* pp. 2049–2054.
- [52] K. Thorborg, *Power electronics, (english translation of kraftelektronik), ny*, (1988).
- [53] C. D. Schauder and R. Caddy, *Current control of voltage-source inverters for fast four-quadrant drive performance*, *IEEE Transactions on Industry Applications* **2**, 163 (1982).
- [54] C. Schauder and H. Mehta, *Vector analysis and control of advanced static var compensators*, in *IEE Proceedings C-Generation, Transmission and Distribution*, Vol. 140 (IET, 1993) pp. 299–306.
- [55] A. Yazdani and R. Iravani, *Voltage-sourced converters in power systems: modeling, control, and applications* (John Wiley & Sons, 2010).
- [56] A. Yazdani01, *Control of an islanded distributed energy resource unit with load compensating feed-forward*, in *Power and Energy Society General Meeting - Conversion and Delivery of Electrical Energy in the 21st Century, 2008 IEEE* (2008) pp. 1–7.
- [57] S.-I. Jang and K.-H. Kim, *An islanding detection method for distributed generations using voltage unbalance and total harmonic distortion of current*, *IEEE transactions on power delivery* **19**, 745 (2004).
- [58] I. PVPS, *Evaluation of islanding detection methods for photovoltaic utility-interactive power systems*, Report IEA PVPS T5-09 (2002).
- [59] H. Zeineldin and J. L. Kirtley, *A simple technique for islanding detection with negligible nondetection zone*, *IEEE Transactions on Power Delivery* **24**, 779 (2009).
- [60] T. Basso, *Ieee standard for interconnecting distributed resources with the electric power system*, in *IEEE Pes Meeting* (2004) p. 1.
- [61] M. A. S. Gaikwad, M. C. M. Reddy, and P. S. Gulhane, *Developing islanding detection arrangement for grid on sensing voltage or frequency variation*, .